Remote Sensing of Environment 279 (2022) 113113

Contents lists available at ScienceDirect

Remote Sensing of Environment

journal homepage: www.elsevier.com/locate/rse

Multi-frequency radiometer-based soil moisture retrieval and algorithm parameterization using in situ sites

Y. Gao [a,1], A. Colliander [b,*], M.S. Burgin [b], J.P. Walker [c], E. Dinnat [d,n], C. Chae [b], M.H. Cosh [e], T.G. Caldwell [f], A. Berg [g], J. Martinez-Fernandez [h], M. Seyfried [i], P.J. Starks [j], D.D. Bosch [k], H. McNairn [l], Z. Su [m], R. van der Velde [m]

[a] Joint Institute for Regional Earth System Science and Engineering, University of California, Los Angeles, Los Angeles, CA 90095, USA
[b] NASA Jet Propulsion Laboratory, California Institute of Technology, Pasadena, CA 91109, USA
[c] Department of Civil Engineering, Monash University, Clayton, VIC 3168, Australia
[d] NASA Goddard Space Flight Center, Greenbelt, MD 20771, USA
[e] USDA Agricultural Research Service, Beltsville, MD 20705, USA
[f] Jackson School of Geosciences, The University of Texas at Austin, Austin, TX 78712, USA
[g] Department of Geography, Environment and Geomatics, University of Guelph, Guelph, ON N1G 2W1, Canada
[h] Instituto Hispano Luso de Investigaciones Agrarias (CIALE), Universidad de Salamanca, Salamanca 37185, Spain
[i] USDA ARS Northwest Watershed Management Research, Boise, ID 83712, USA
[j] USDA ARS Grazinglands Research Laboratory, El Reno, OK 73036, USA
[k] USDA ARS Southeast Watershed Research Laboratory, Tifton, GA 31793, USA
[l] Agriculture and Agri-food Canada, Ontario K1A 0C6, Canada
[m] University of Twente, 7500 AE Enschede, the Netherlands
[n] Center of Excellence in Earth Systems Modelling and Observations, Chapman University, Orange, CA 92866, USA

ARTICLE INFO

Edited by Jing M. Chen

Keywords:
Passive microwave
Radiometer
Soil moisture
Parameterization
Calibration

ABSTRACT

L-band brightness temperature (TB) has been shown to provide the best sensitivity to soil moisture (SM) although C- and X-band based products offer a longer time-series from satellite-based measurements. Currently, global coverage SM is routinely produced from spaceborne measurements using all three frequency bands, but despite continued validation efforts of the products, the relative characteristics and performance of these observations have not been fully established. Therefore, this study focused on the parametrization of SM retrieval algorithms at L-, C- and X-bands using TB observations from the L-band radiometer on NASA's SM Active Passive (SMAP) mission and the C- and X-band channels of JAXA's Advanced Microwave Scanning Radiometer 2 (AMSR2) on-board the GCOM-W satellite. These can be applied in global SM retrieval algorithms using either one of the frequencies or a combination of them. The reference in situ SM data was obtained from 12 core validation sites across various land cover types around the world. The investigation highlighted the known challenges of retrieving SM from C- and X-band data compared to the higher sensitivity of the L-band data. Even with a site-specific retrieval algorithm parameterization, the mean correlation of the C- and X-band retrievals for the core validation site SM measurement were much lower than that for L-band, being 0.52 (0.54) and 0.45 (0.47) for vertical (horizontal) polarization, respectively, while for the L-band retrieval the corresponding values were 0.81 (0.77). The parameterization exercise showed that matching the C- and X-band TB measurements with an emission model was not difficult; the problem was relating the observations to SM under the influence of large roughness and vegetation effects. As a result, parameter optimization produced values for some sites that were not realistic or did not allow any practical sensitivity to SM at C- and X-band. Considering the L-band observations, the parameter optimization resulted in superior bias performance as compared to the operational SMAP

* Corresponding author.
E-mail addresses: ying.gao@monash.edu (Y. Gao), Andreas.Colliander@jpl.nasa.gov (A. Colliander), Mariko.S.Burgin@jpl.nasa.gov (M.S. Burgin), jeff.walker@monash.edu (J.P. Walker), Emmanuel.Dinnat@nasa.gov (E. Dinnat), Chun.Sik.Chae@jpl.nasa.gov (C. Chae), Michael.Cosh@ars.usda.gov (M.H. Cosh), tcaldwell@usgs.gov (T.G. Caldwell), aberg@uoguelph.ca (A. Berg), jmf@usal.es (J. Martinez-Fernandez), mark.seyfried@ars.usda.gov (M. Seyfried), patrick.starks@ars.usda.gov (P.J. Starks), David.Bosch@ars.usda.gov (D.D. Bosch), heather.mcnairn@agr.gc.ca (H. McNairn), z.su@utwente.nl (Z. Su), r.vandervelde@utwente.nl (R. van der Velde).
[1] Now is with Department of Civil Engineering, Monash University, Clayton, VIC 3168, Australia.

https://doi.org/10.1016/j.rse.2022.113113
Received 16 December 2021; Received in revised form 1 May 2022; Accepted 4 June 2022
Available online 21 June 2022

product parameterization, but the sensitivity to SM changes (R and unbiased root mean square difference) did not improve markedly, or in some cases degraded at the expense of a smaller bias.

1. Introduction

Soil moisture (SM) is a key variable in the energy exchange and water balance of Earth's land-atmosphere system. It is of great importance to disciplines such as agriculture, hydrology, and meteorology. Over the past twenty years, passive microwave remote sensing has grown into a popular technique to estimate surface SM at a global scale. A number of launched satellite missions with onboard radiometers have the ability for a global SM mapping. The National Aeronautics and Space Administration (NASA) launched the Advanced Microwave Scanning Radiometer-EOS (AMSR-E) developed by Japan Aerospace Exploration Agency (JAXA) on the Aqua spacecraft in May 2002 (Njoku et al., 2003) (operation ceased in October 2011). The European Space Agency (ESA) launched the Soil Moisture and Ocean Salinity (SMOS) mission in November 2009 (Kerr et al., 2010). After that, the Advanced Microwave Scanning Radiometer 2 (AMSR2) developed by JAXA and onboard the Global Change Observation Mission-Water (GCOM-W) satellite was launched in May 2012 (Imaoka et al., 2010). Most recently, NASA's Soil Moisture Active Passive (SMAP) mission was launched in January 2015 (Entekhabi et al., 2010). The instrument specifications related to SM mapping capabilities for these missions are shown in Table 1.

SM retrieved from passive microwave observations has been applied for a range of different purposes. However, products from different missions have typically been used separately, which limits the length of the available SM time-series. SM data acquired from various missions with different algorithms or model parameters differ in their characteristics and are therefore not consistent. Parinussa et al. (2015) conducted an analysis towards consistent AMSR2 SM products. The global SM, retrieved from C−/X-band signals, was compared against ERA-interim SM (a global land surface reanalysis data set), indicating the need for inter-calibration between different frequencies. It is also suggested that using such products while making assumptions for the sensing depth, which varies among different frequencies, is quite typical. There have been also efforts to develop joint SM products from different missions. The ESA Climate Change Initiative SM product uses statistical methods to merge SM products. However, the validation showed that the consistency of the product requires improvements (Dorigo et al., 2017). Therefore, we conducted a study using the L-, C- and X-band signals from SMAP and AMSR2 satellites to explore the consistency of the SM model parameterization over frequency.

The behavior of the TB signal in response to SM change and vegetation cover has been widely characterized in many previous studies at different frequencies based on field experiment data (e.g., Burke et al., 1979; Wigneron et al., 1995; Jackson et al., 2002; Jackson and O'Neill, 1990; Njoku et al., 2002). Schmugge et al. (1986) concluded that L-band gives the optimum frequency range for SM retrieval. The higher frequencies, however, have been also explored as they " require a smaller antenna aperture to achieve equal spatial resolution" (Njoku et al., 2003). At L-band, the brightness temperature (TB) signal originates from about the top 5 cm of soil surface on average (e.g., Njoku and Kong, 1977). O'Neill et al. (1996) showed that with a corn crop coverage of no >5 kg/m^2 of water content (i.e., a moderate vegetation cover), L-band radiometry can achieve a SM retrieval accuracy as good as 0.04 m^3/m^3; this threshold has been widely used in the development of SM products (e.g., Entekhabi et al., 2014), but it has not been tested across most of the vegetation types. On the other hand, higher frequency radiometers (e.g., those at C-band or X-band) have higher attenuation through vegetation and smaller penetration depth. Unlike L-band, TB observed at C- and X-band is only representing the top 1 cm of the soil surface or even less (e.g., Njoku and Kong, 1977). A vegetation water content (VWC) value of higher than ~3 kg/m^2 would attenuate the signal enough so that it is not sensitive to SM.

Before L-band was available from satellite sensors, algorithm research for satellite-based global retrievals focused on higher-frequency observations. For example, Njoku and Li (1999) proposed an approach using C-, X- and Ku-band observations to retrieve SM, vegetation water content and surface temperature, and Paloscia et al. (2001) developed a multi-frequency approach using C-band for SM retrieval, while accounting for vegetation effects with X-band signals from SMMR and SSM/I satellites. More recently, there have also been studies on multi-frequency SM retrievals after the launch of SMOS and SMAP. For example, Chai et al. (2018) conducted a case study over corn fields with a "multi-band (1.4/6.925/10.65 GHz) emission model", which accounts for the multiple-scattering effects in the matrix doubling model. Results provide overall RMSEs of <8 K at all three frequencies against both ground and airborne observations. van der Schalie et al. (2018) quantified the consistency between AMSR-E and SMOS-based SM retrievals from various retrieval algorithms over a global comparison study. Results showed that the two missions have similar behavior over sparse to moderately vegetated land. Conversely, Crow et al. (2017) and Dong and Crow (2018) showed that the L-band radiometry-based SM products had a significant advantage over higher-frequency-based products for predicting rain runoff and coupling SM with air temperature extremes because of the better sensitivity to SM.

This paper presents the parameterization of the Single Channel Algorithm (SCA) (O'Neill et al., 2021), which uses the tau-omega model (Mo et al., 1982) to characterize the vegetation layer and single parameter roughness model to characterize surface roughness effect (Choudhury et al., 1979). The tau-omega model has been used in both SMAP and SMOS missions at L-band (Entekhabi et al., 2010; Kerr et al., 2012) and has also been applied to AMSR2 and AMSR-E at X-band (Mladenova et al., 2014). Van de Griend and Wigneron (2004) demonstrated that the vegetation parameter b (which characterizes tau, see Section III) is inversely proportional to the power of the wavelength when considering a wide frequency range. However, that study was based on results from individual data collected separately at different times and locations. In this study, we use almost 3 years (2015–2017) of continuous TB observations at L-, C- and X-band over 12 validation sites around the world to further explore the frequency dependence of the vegetation and surface roughness parameters. SMAP and AMSR2 TB observations that cover a range of SM-sensitive frequencies from 1.4 to 10.6 GHz were applied. The in situ monitoring sites are used to calibrate and validate the surface roughness and vegetation parameters of the forward model at different frequencies. Unlike SMAP, which has established a set of default model parameters presented in its Algorithm Theoretical Basis Document (ATBD) (O'Neill et al., 2021), such parameters are not readily available for AMSR2. Therefore, this study

Table 1
Instrument description for satellite missions with passive microwave radiometers that have global soil moisture mapping capabilities.

Mission	Available data	Frequency in GHz (Band)	Spatial resolution in kms	Incidence angle in degrees	Temporal revisit
AMSR-E	2002–2011	6.93 (C) 10.65 (X)	75 × 43 51 × 29	55	~2 days
SMOS	2009-present	1.41 (L)	30–80	0–55	~3 days
AMSR2	2012-present	6.93 (C) 7.30 (C) 10.65 (X)	62 × 35 62 × 35 42 × 24	55	~2 days
SMAP	2015-present	1.41 (L)	38 × 49	40	~3 days

Table 2
IGBP-based Percentage of Cropland and Grassland for in situ sites, together with ancillary input tau-omega model parameters for calibration.

Site	Location	Cropland %	Grassland %	Clay %	Sand %	ρ (kg/m^3)	Q (L)	Q (C, X)	ω (L)	ω (C, X)
Croplands										
Carman	Canada	99.7	–	31.4	29.9	1.18	0	0.05	0.05	0.08
Kenaston	Canada	98.8	1.2	23.2	32.3	1.22				
REMEDHUS	Spain	82.5	0.3	33.6	28.0	1.38				
South Fork	USA	99.9	–	37.9	30.8	1.34				
Grasslands										
Little Washita	USA	20.8 *	65.7 *	16.4	52.8	1.44	0	0.05	0.05	0.06
Reynolds Creek	USA	1.2	95.0	37.5	25.7	1.41				
TxSON	USA	0.6	83.4	30.7	36.9	1.43				
Mixed										
Fort Cobb	USA	52.0 *	33.9 *	18.4	33.3	1.44	0	0.05	0.05	0.08
Kyeamba	Australia	34.5	49.9	17.9	65.8	1.43				
Little River **	USA	19.5	0.1	80.0	7.2	1.47				
Twente ***	The Netherlands	9.2	2.1	8.6	76.0	1.21				
Yanco	Australia	27.1	61.9	37.8	44.1	1.33				

* Numbers are based on local land cover studies done by Starks et al. (2014). The MODIS IGBP classification indicates 5.4% of cropland and 94.2% of grassland at Fort Cobb, and 0.6% of cropland and 98.2% grassland for Little Washita, which show a considerable difference compared to local studies, therefore not considered.
** The dominant landcover for Little River is Cropland/Natural Mosaic, taking up 57.0%; therefore categorized as 'mixed'.
*** The dominant landcover for Twente is Cropland/Natural Mosaic, taking up 66.9%; therefore categorized as 'mixed'.

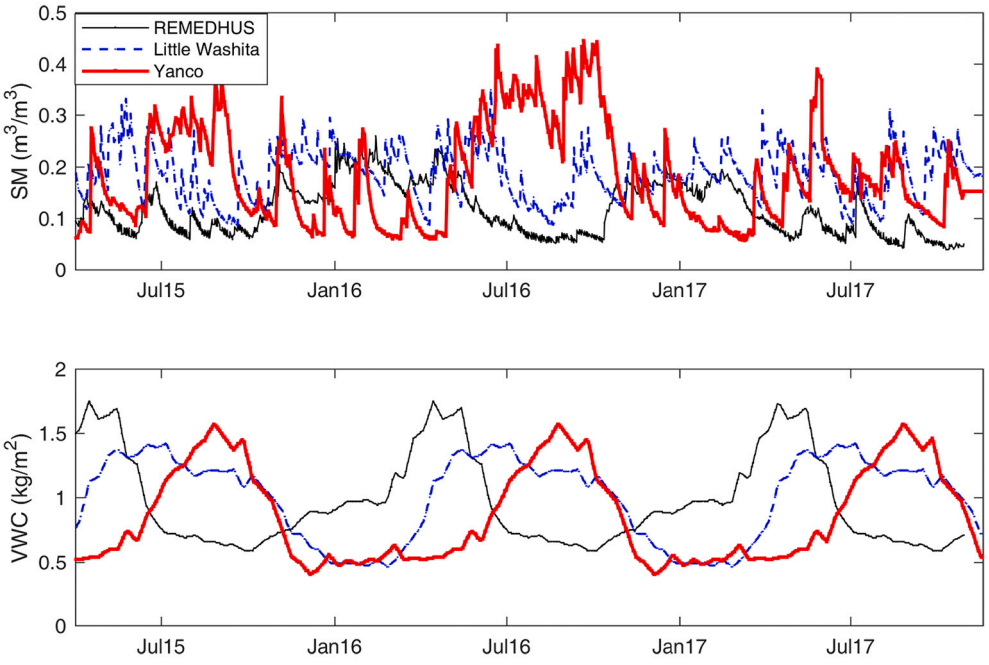

Fig. 1. Time series of soil moisture from in situ monitoring stations (top) and vegetation water content retrieved from MODIS NDVI climatology (bottom) at REMEDHUS, Little Washita and Yanco from April 2015 to December 2017.

proposes tau-omega model parameters to be used in C- and X-band SM retrievals for various landcover types.

2. Data sets

2.1. In situ data

This study focuses on 12 in situ monitoring sites around the world, mostly cropland and grassland sites, to calibrate and validate parameters of the forward model at different frequencies. These are SMAP core validation sites, which satisfy the condition of measuring SM at 5 cm depth continuously with replication over the 36-km SMAP pixel domain (Colliander et al., 2017). In this study, the in situ sites are categorized into three groups: Croplands (Carman (Bhuiyan et al., 2018), Kenaston (Tetlock et al., 2019), REMEDHUS (Martinez-Fernandez and Ceballos, 2005) and South Fork (Coopersmith et al., 2015)), Grasslands (Little Washita (Starks et al., 2014), Reynolds Creek (Seyfried et al., 2018) and TxSON (Caldwell et al., 2019)) and Mixed (Fort Cobb (Starks et al., 2014), Kyeamba (Smith et al., 2012), Little River (Bosch et al., 2007), Twente (van der Velde et al., 2021) and Yanco (Panciera et al., 2014)), based on the International Geosphere–Biosphere Programme (IGBP) landcover classification system. If the cropland percentage exceeds 65% of the SMAP grid area, it is considered a cropland site; the same applies for the grassland category. The Mixed category consists of sites where both cropland and grassland take up a considerable amount of area, or they have other dominant landcover types such as cropland/natural mosaic or mixed forest, etc. The cropland and grassland percentages are summarized in Table 2. Some core validation sites were not included

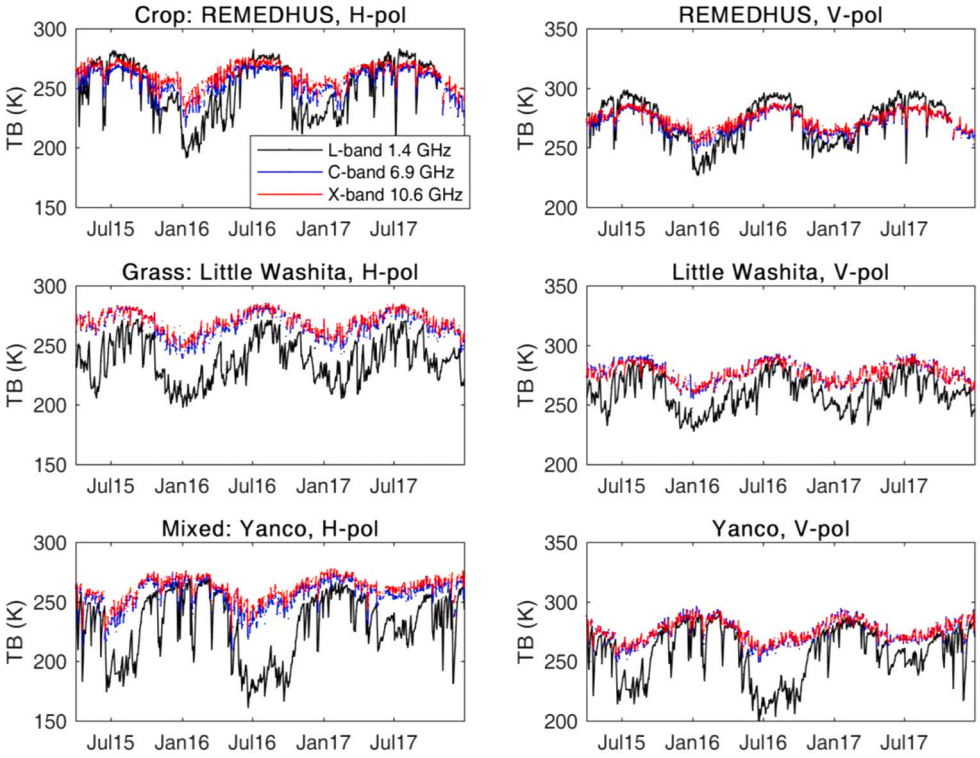

Fig. 2. TB observations at H-pol and V-pol from SMAP (L-band, 1.4 GHz) and AMSR2 (C-band, 6.9 GHz and X-band, 10.6 GHz) at REMEDHUS, Little Washita and Yanco.

because AMSR2 C- and X-band data were scarcely available over these sites. For example, the Walnut Gulch site in Arizona was excluded from the analysis. Table 3 in Colliander et al. (2022) lists information regarding each site.

Fig. 1 shows a time series of SM and vegetation water content (VWC) at one example site for each category: REMEDHUS for croplands, Little Washita for grasslands, and Yanco for mixed, over the study period April 2015 to end of 2017. The SM was logged by in situ monitoring stations located within each network and then aggregated to the satellite footprint with the "Voronoi Diagram method", as explained in Colliander et al. (2017). The VWC was retrieved from a NDVI (Normalized Difference Vegetation Index) climatology derived from MODIS (Moderate Resolution Imaging Spectroradiometer) data, which is also used as ancillary data in the SMAP passive SM retrieval algorithm (see Section II·B). Yanco has the most significant seasonal variation for SM which peaks in the wet season of the southern-hemispheric winter. REMEDHUS has some seasonal variabilities, but within a smaller range compared to Yanco. Little Washita, however, has no clear seasonal trend during this period. All three sites have obvious seasonal variability for VWC which peak in different times of year. The NDVI climatology represents the average of 10 years of NDVI data; therefore, the retrieved VWC time series shown here are not the actual VWC for each site and are expected to be less fluctuating in terms of seasonal variation as compared with actual VWC.

2.2. Satellite data

SMAP's L-band radiometer at 1.41 GHz measures TB at a 40° incidence angle (Entekhabi et al., 2010). It provides 38-km spatial resolution with the projection of 3-dB antenna footprint (Piepmeier et al., 2017). AMSR2 instrument measures TB at six frequencies, ranging from 6.93 to 89 GHz. It applies conical scanning with an incidence angle of 55°. The AMSR2 single-channel SM retrieval algorithm utilizes the 10.65 GHz (X-band) frequency channel to retrieve SM. Although the 6.93 GHz (C-band) frequency can be affected by radio frequency interference (RFI) (Imaoka et al., 2010), it does have SM retrieval capability and RFI was not observed during our study period within the 12 chosen study sites. Therefore, both C-band and X-band observations from AMSR2 are considered in the analysis of this study.

The SMAP enhanced SM product (L2SMPE, Version 1) provided the L-band TB observations for each 33 km × 33 km pixel over the in situ sites (Chan et al., 2018; Colliander et al., 2018). The AMSR2 TB product (standard L1B version 2 product with raw resolution) provided the C- and X-band TB observations. The product was subsequently re-sampled to the same pixel resolution as SMAP over the 12 sites. Only the morning overpasses are considered for both SMAP and AMSR2 for the purpose of consistency, because the temperature differences between the top and deeper layers of soil as well as between vegetation and soil are smaller in the morning compared to the afternoon (O'Neill et al., 2021). The product uses VWC as an ancillary input parameter, which is based on a 10-year NDVI climatology from MODIS. The VWC for the global scale is derived using a set of land cover-based equations (O'Neill et al., 2021). Herein, this VWC was used over each core site as an input parameter for the tuning process.

Fig. 2 shows the TB variation for REMEDHUS, Little Washita and Yanco at H-pol and V-pol throughout the study period. It is clear that L-band data has a significantly larger dynamic range than C- and X-band that almost overlap with each other. C- and X-band TBs also have a relatively consistent and gentle seasonal variability throughout the study period, while L-band has a stronger variation. For example, around January 2016 and hence during summer in the Southern hemisphere, TB H-pol for Yanco at the three frequencies are almost at the same level of ~270 K, except that L-band has several sharp spikes in response to short rainfall events. When entering the winter season around July 2016, however, C- and X-band decrease slightly to ~250 K while L-band drops dramatically to <180 K.

Fig. 3 shows the scatter plots of C- and X-band data against L-band. For higher TB or drier conditions, C- and X-band signals are very close to L-band. However, the difference becomes larger when TB decreases or conditions gets wetter. Overall, V-pol is more condensed and less

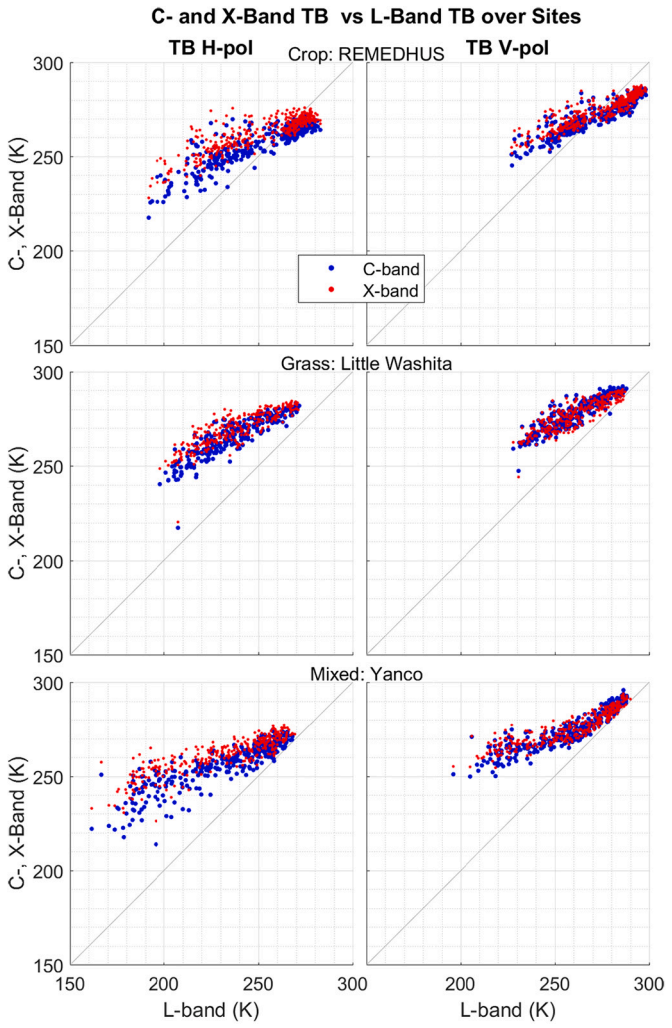

Fig. 3. Scatter plots of TB observations at H-pol and V-pol from SMAP (L-band, 1.4 GHz) and AMSR2 (C-band, 6.9 GHz and X-band, 10.6 GHz) at REMEDHUS, Little Washita and Yanco.

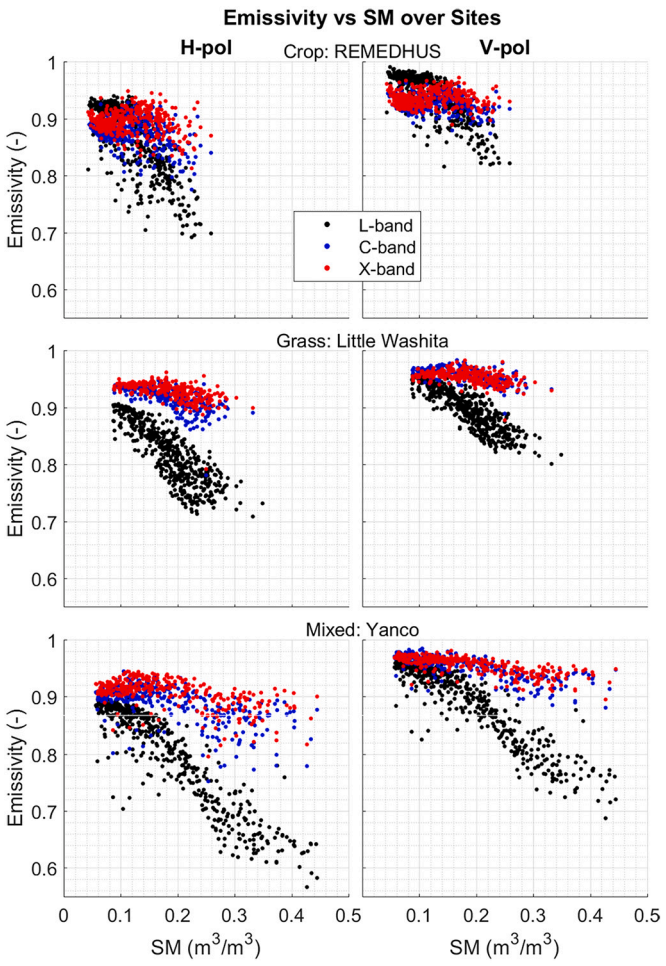

Fig. 4. Scatter plots of surface emissivity (TB/T_{SURF}) against in situ soil moisture at L-, C- and X-band at H-pol and V-pol for REMEDHUS, Little Washita and Yanco.

scattered than H-pol signals.

With soil surface temperature (T_{SURF}) available from in situ monitoring networks (the observation depth is 5 cm below the surface), the surface emissivity can be estimated by TB/T_{SURF}. Ideally, the emissivity is computed using the effective temperature (e.g., Njoku and Kong., 1977) accounting for the effects of vegetation and penetration into soil; both of which are functions of frequency. Here we had only the soil temperature measurement from one depth for each site so the estimation of the effective temperature would have substantial uncertainties, and the simple soil temperature-based estimate can give a useful indication of the first-order trends of emissivity. In order to show the sensitivity of signals at each frequency to SM, the surface emissivity is plotted against in situ SM at L-, C- and X-band in Fig. 4. As expected, the L-band signal has the steepest slope and hence the highest sensitivity to SM; the C- and X-band signals exhibit a much flatter signature as compared to L-band, indicating lower sensitivity to SM. Fig. 5 shows simulated emissivity for a smooth, bare surface using the Mironov soil dielectric model (Mironov et al., 2009), the Fresnel equation (as is done in the SCA), and the incidence angles corresponding to the SMAP and AMSR2 observations. The frequency dependent differences in these plots are mostly due to the incidence angle difference while the effect by the soil dielectric model is relatively small. For the H-polarization the slope is similar for the L-band TB and the C/X-band TB, but there is a substantial offset between them. For the V-polarization, the emissivity range extends closer to unity, where L-band and C/X-band values have to come closer together. Compared to the measured frequency dependent differences in Fig. 3, the simulated V-polarization trends have similarities with the measured trends which may be because of the closeness to unity, but for the H-polarization the trends are clearly different. The simulated emissivity of the different frequencies exhibit similar slope with an offset, but for the measured values the slope between the frequencies is clearly different suggesting that the observed differences are mostly due to the frequency dependency of the roughness and vegetation effects (at least within the SCA framework). The higher sensitivity to surface roughness and vegetation subdued the impact of the high soil dielectric constant resulting in a smaller observed range of emissivity.

The differences in sensing depth (which also affect the effective soil temperature, e.g. Lv et al., 2014) do not cause the systematic and large differences. If the sensing depth was the main cause, the smallest differences would be observed at the wet end (when the penetration depths become more similar) and the largest at the dry end (when a possibly varying SM profile would affect more the lower frequency measurements). Furthermore, the use of the same soil surface temperature for each frequency to represent effective temperature cannot be the source of the differences, because that would require an adjustment of tens of degrees, which is not realistic. When comparing among different sites in Fig. 4, REMEDHUS appears to be more scattered and noisier than Yanco and Little Washita. This is likely due to the larger dynamic range of VWC at REMEDHUS which contributes to a 'widening' of the relationship curve. Yanco has the 'longest' curve among the three sites, which is due

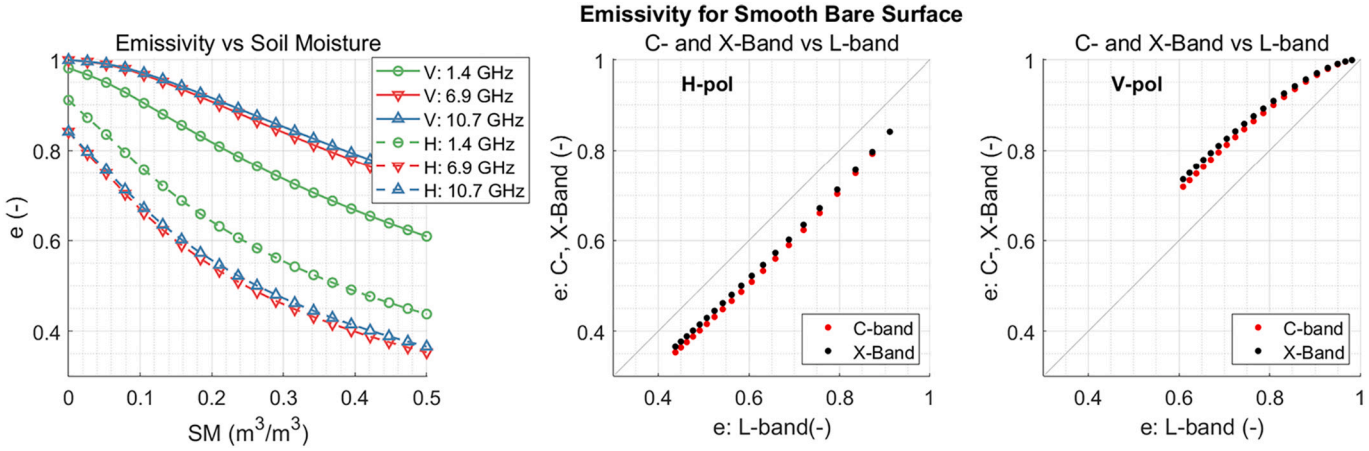

Fig. 5. Simulated emissivity for smooth bare surface for L-band (at 40° incidence angle), and C- and X-band (at 55° incidence angle). (Left) Emissivity as a function of soil moisture; (Middle) and (Right) C- and X-band emissivity as a function of L-band emissivity for V-polarization and H-polarization, respectively.

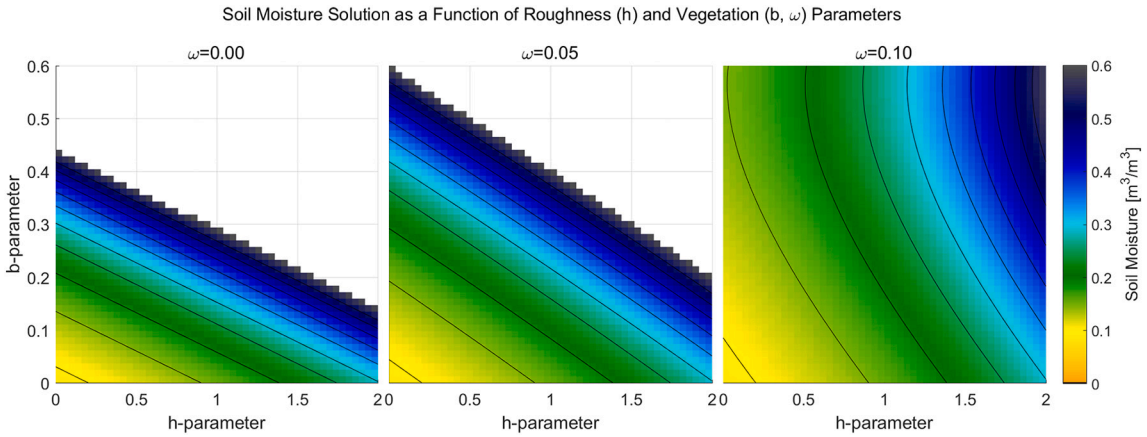

Fig. 6. Soil moisture solutions as a function of h, b and ω parameters for TB = 270 K and VWC = 1.5 kg/m^2.

to the largest dynamic range of SM.

3. Methodology

The SM retrieval and model parameterization process are divided into two stages: In stage 1, TB data from April 2015 to December 2016 is used for model calibration against in situ SM for L-, C- and X-band, respectively. In stage 2, data from January to December 2017 is used for validation of the calibrated parameters (only thawed conditions are considered). The SMAP default parameters will also be applied to compare against the calibrated parameters at L-band.

As its name suggests, the concept of tau-omega model relies on two parameters (Mo et al. (1982)): 1) canopy optical depth (τ) to characterize vegetation attenuation and 2) single-scattering albedo (ω) to parameterize the scattering effects within the canopy layer. Parameter τ was found to be linearly related to VWC through parameter b: $\tau = b \times$ VWC, where the value of b depends on vegetation and frequency (Jackson and Schmugge, 1991). The temperature of the vegetation canopy required in the model can be assumed equal to the soil surface temperature during the satellite morning overpass. In the SCA framework, the surface roughness is accounted through a single parameter (h) using the formulation first introduced in Choudhury et al. (1979). The detailed description of SCA used in this study can be found in O'Neill et al. (2021).

There have been a large number of studies regarding the parameterization of SCA; in particularly for L-band, resulting in a range of roughness and vegetation parameters (e.g., Choudhury et al., 1979; Mo et al., 1982; Jackson et al., 1999; Wigneron et al., 2001, 2011, 2017; Fernandez-Moran et al., 2017). Colliander et al. (2016) summarized the roughness parameter values reported for L-band in 11 studies, ranging from 0.06 to 1.13. Ulaby and Wilson (1985) developed a vegetation attenuation model as a function of frequency for L-, C- and X-band based on field measurements, which was translated to a function of b in Jackson and Schmugge (1991). Table 1 in Jackson and Schmugge (1991) lists b-parameters for L-, C- and X-band from a number of studies including a mix of vegetation types; the average values for the frequency bands are 0.11 ± 0.03, 0.20 ± 0.10 and 0.68 ± 0.39 (excluding the one outlier study), respectively. Jackson and Schmugge (1991) applied $b = b'\lambda^x$ to represent the frequency dependency of b, where b' is a frequency-independent parameter, λ is the wavelength, and x is determined empirically. Depending on the vegetation type and frequency range, the value of x ranged from −1.5 to −0.5 when the equation was applied in Kirdiashev et al. (1979), Ulaby and Wilson (1985), Pampaloni and Paloscia (1986), and Jackson and Schmugge (1991).

The examples above demonstrate the wide range of parameters used for SCA-type models. As many of the values were obtained by tuning an SCA-type model, an important underlying factor contributing to the wide range is the coupling of the h, b and ω parameters in the SCA model. This means that the same SM value can be reached from multiple TB values with different combinations of the parameters. We further explored the relationship of the h, b and ω parameters to the SM solution using the SCA with a fixed TB (270 K) and VWC (1.5 kg/m^2) values.

Table 3
Calibrated b and h, Calibration statistics of retrieved against in situ soil moisture and Retrieval statistics using SMAP default b and h over core validation sites for 2015–2016 time period (bold numbers Indicate the best performance for each polarizations and red numbers indicate the better of the two polarizations).

Band, pol	b	h	RMSD	Mean Dif.	ub. RMSD	R	Band, pol	b	h	RMSD	Mean Dif.	ub. RMSD	R
CARMAN (Crop)							KENASTON (Crop)						
SMAP, H	*0.110*	*0.108*	*0.112*	*−0.067*	***0.090***	***0.37***	*SMAP, H*	*0.110*	*0.109*	*0.057*	*−0.043*	*0.037*	*0.74*
L-band, H	0.10	0.21	**0.110**	**−0.062**	0.091	**0.37**	L-band, H	0.03	0.91	**0.036**	**−0.005**	**0.035**	**0.76**
C-band, H	0.12	1.61	0.166	−0.118	0.117	0.17	C-band, H	0.13	2.31	0.067	−0.034	0.058	0.46
X-band, H	0.12	1.95	0.172	−0.123	0.120	0.15	X-band, H	0.13	2.80	0.074	−0.041	0.062	0.44
SMAP, V	*0.110*	*0.108*	*0.094*	*−0.060*	***0.073***	***0.43***	*SMAP, V*	*0.110*	*0.109*	*0.036*	*−0.024*	***0.029***	***0.76***
L-band, V	0.12	0.19	0.092	−0.044	0.080	**0.43**	L-band, V	0.03	0.78	**0.029**	**−0.002**	**0.029**	0.71
C-band, V	0.12	0.65	**0.088**	**−0.032**	0.082	0.29	C-band, V	0.03	0.92	0.030	**−0.002**	0.030	0.65
X-band, V	0.12	0.71	0.095	−0.039	0.087	0.23	X-band, V	0.03	0.92	0.032	−0.008	0.031	0.60
REMEDHUS (Crop)							**SOUTH FORK (Crop)**						
SMAP, H	*0.110*	*0.109*	*0.040*	*−0.022*	***0.034***	***0.90***	*SMAP, H*	*0.110*	*0.108*	*0.105*	*−0.078*	***0.070***	***0.59***
L-band, H	0.03	0.51	**0.037**	−0.013	0.035	0.89	L-band, H	0.10	0.31	**0.101**	**0.059**	0.082	0.56
C-band, H	0.15	1.62	0.040	**−0.008**	0.039	0.68	C-band, H	0.10	1.81	0.165	−0.123	0.111	0.42
X-band, H	0.17	2.07	0.047	**−0.008**	0.047	0.55	X-band, H	0.10	2.17	0.159	−0.105	0.120	0.40
SMAP, V	*0.110*	*0.109*	*0.037*	***−0.007***	*0.037*	***0.89***	*SMAP, V*	*0.110*	*0.108*	*0.090*	*−0.074*	***0.051***	*0.63*
L-band, V	0.03	0.26	**0.033**	−0.010	**0.031**	0.88	L-band, V	0.11	0.46	**0.076**	−0.039	0.065	**0.64**
C-band, V	0.03	0.26	0.075	0.062	0.044	0.50	C-band, V	0.11	0.83	0.085	−0.031	0.079	0.43
X-band, V	0.03	0.26	0.070	0.052	0.047	0.35	X-band, V	0.11	0.83	0.092	**−0.013**	0.091	0.38
LITTLE WASHITA (Grass)							**REYNOLDS CREEK (Grass)**						
SMAP, H	*0.130*	*0.155*	*0.064*	*−0.059*	***0.026***	***0.89***	*SMAP, H*	*0.129*	*0.155*	*0.067*	*−0.056*	***0.037***	*0.66*
L-band, H	0.07	0.81	**0.046**	−0.019	0.042	**0.89**	L-band, H	0.02	1.10	**0.055**	−0.012	0.054	**0.72**
C-band, H	0.12	3.78	0.051	**−0.018**	0.048	0.72	C-band, H	0.12	2.70	0.075	−0.005	0.074	0.38
X-band, H	0.14	3.84	0.058	−0.038	0.044	0.67	X-band, H	0.12	2.80	0.079	**−0.003**	0.079	0.20
SMAP, V	*0.130*	*0.155*	*0.034*	*−0.025*	***0.024***	***0.92***	*SMAP, V*	*0.129*	*0.155*	*0.058*	*−0.040*	***0.042***	*0.67*
L-band, V	0.05	0.76	**0.032**	−0.011	0.030	**0.92**	L-band, V	0.02	0.98	**0.052**	**−0.011**	0.051	**0.74**
C-band, V	0.05	1.65	0.042	**−0.003**	0.042	0.62	C-band, V	0.02	0.98	0.102	0.067	0.076	0.25
X-band, V	0.05	1.65	0.047	0.011	0.045	0.54	X-band, V	0.02	0.98	0.111	0.079	0.079	0.09
TxSON (Grass)							**FORT COBB (Mixed)**						
SMAP, H	*0.127*	*0.153*	*0.083*	*−0.081*	***0.021***	***0.96***	*SMAP, H*	*0.129*	*0.153*	*0.090*	*−0.083*	***0.035***	*0.84*
L-band, H	0.08	0.78	**0.024**	**−0.006**	0.023	0.94	L-band, H	0.03	0.92	**0.057**	**−0.027**	0.050	**0.85**
C-band, H	0.21	3.10	0.085	−0.024	0.081	0.42	C-band, H	0.10	3.60	0.100	−0.052	0.086	0.59
X-band, H	0.21	3.80	0.094	−0.022	0.092	0.27	X-band, H	0.10	3.92	0.103	−0.051	0.089	0.53
SMAP, V	*0.127*	*0.153*	*0.042*	*−0.038*	***0.018***	***0.97***	*SMAP, V*	*0.129*	*0.153*	*0.063*	*−0.056*	***0.029***	*0.87*
L-band, V	0.10	0.42	**0.020**	0.003	0.020	0.95	L-band, V	0.02	0.92	**0.040**	−0.013	0.038	**0.88**
C-band, V	0.10	1.16	0.070	**0.000**	0.070	0.46	C-band, V	0.03	2.30	0.054	−0.012	0.053	0.49
X-band, V	0.10	1.24	0.077	−0.003	0.077	0.27	X-band, V	0.03	2.30	0.055	**0.005**	0.054	0.44
KYEAMBA (Mixed)							**LITTLE RIVER (Mixed)**						
SMAP, H	*0.120*	*0.135*	*0.184*	*0.097*	*0.160*	***0.88***	*SMAP, H*	*0.110*	*0.127*	*0.055*	*0.026*	*0.048*	***0.84***
L-band, H	0.02	0.56	**0.060**	**−0.014**	**0.058**	**0.88**	L-band, H	0.02	1.04	**0.045**	**0.007**	**0.044**	0.81
C-band, H	0.12	2.75	0.128	−0.047	0.119	0.52	C-band, H	0.09	2.20	0.069	−0.026	0.062	0.56
X-band, H	0.12	3.15	0.121	−0.049	0.111	0.50	X-band, H	0.09	2.64	0.071	−0.025	0.064	0.50
SMAP, V	*0.120*	*0.135*	*0.119*	*0.067*	*0.099*	***0.92***	*SMAP, V*	*0.110*	*0.127*	*0.072*	*0.062*	*0.036*	***0.86***
L-band, V	0.02	0.41	**0.048**	−0.004	**0.048**	0.91	L-band, V	0.02	0.60	**0.030**	0.008	**0.029**	0.85
C-band, V	0.05	1.56	0.104	**−0.002**	0.104	0.49	C-band, V	0.02	1.00	0.051	0.005	0.050	0.40
X-band, V	0.05	1.56	0.110	0.016	0.109	0.41	X-band, V	0.02	1.00	0.053	**0.001**	0.053	0.31
TWENTE (Mixed)							**YANCO (Mixed)**						
SMAP, H	*0.110*	*0.120*	*0.121*	*0.053*	*0.109*	*0.83*	*SMAP, H*	*0.122*	*0.138*	*0.063*	*0.013*	*0.061*	***0.95***
L-band, H	0.02	1.11	**0.063**	**−0.027**	**0.057**	**0.86**	L-band, H	0.06	0.24	**0.038**	**−0.011**	**0.036**	**0.95**
C-band, H	0.04	3.08	0.078	−0.035	0.070	0.74	C-band, H	0.30	0.72	0.098	−0.069	0.069	0.79
X-band, H	0.04	3.57	0.080	−0.034	0.073	0.69	X-band, H	0.30	1.36	0.102	−0.071	0.075	0.74
SMAP, V	0.110	0.120	0.075	0.038	0.065	0.87	SMAP, V	0.122	0.138	0.056	0.029	0.047	**0.96**
L-band, V	0.02	1.00	**0.040**	−0.009	**0.039**	**0.88**	L-band, V	0.06	0.06	**0.031**	**−0.003**	**0.031**	**0.96**
C-band, V	0.04	1.06	0.059	**0.000**	0.059	0.53	C-band, V	0.12	1.10	0.073	0.029	0.068	0.70
X-band, V	0.04	1.45	0.066	−0.003	0.066	0.38	X-band, V	0.12	1.22	0.079	0.031	0.073	0.64

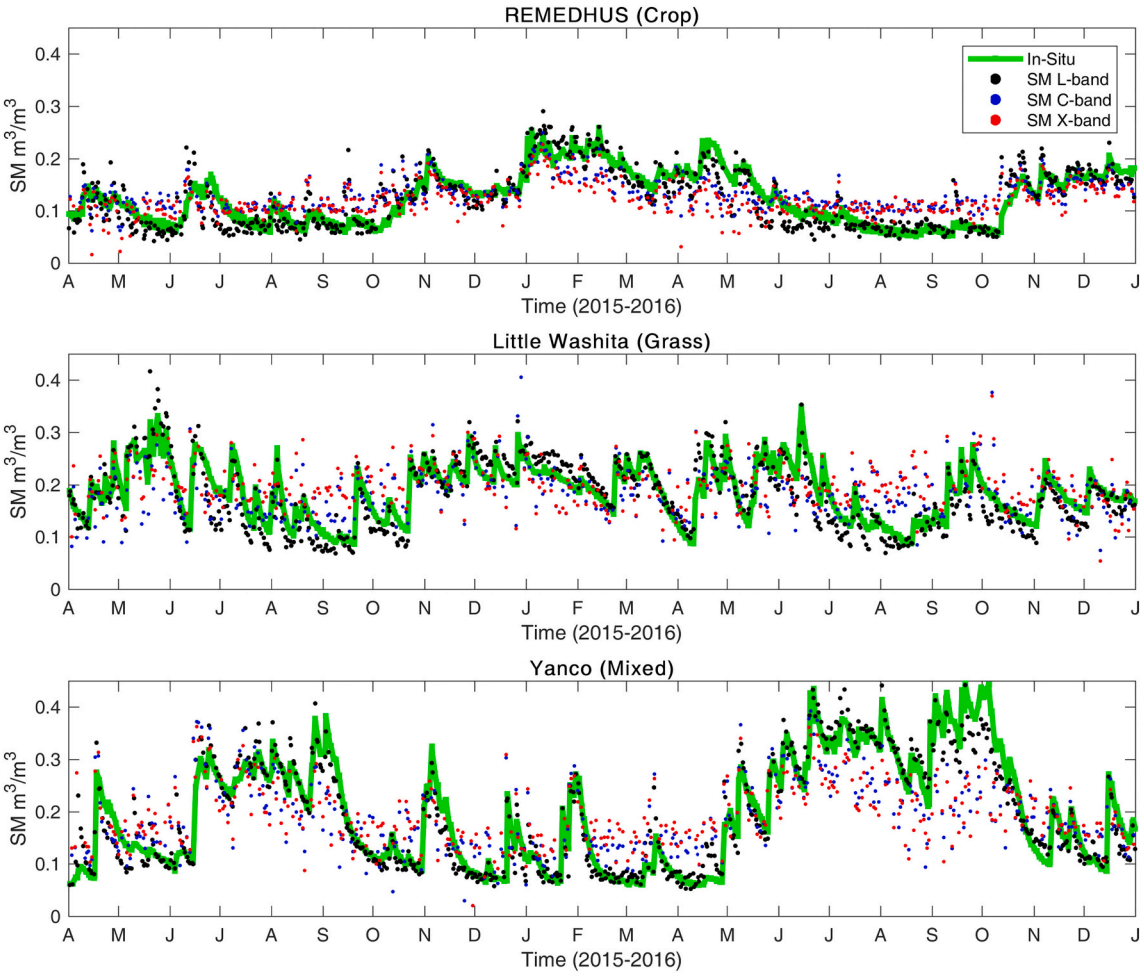

Fig. 7. Soil moisture retrieval using the calibrated forward model parameters at L-band, C-band and X-band at V-pol together with soil moisture 'truth' from in situ monitoring stations at REMEDHUS, Little Washita and Yanco from April 2015 to December 2016.

Fig. 6 shows the SM as a function of h and b parameters for three values of ω. The isovalue contours highlight the range of b and h parameter values that result in the same SM solution. This is further exemplified by comparison with the parameterization used in Jackson et al. (2002) and Bindlish et al. (2006) for retrieving SM using an airborne C-band radiometer. The former used an h-parameter of 0.3 for grass and 0.6 for stubble, which resulted in $b = 0.75$ for both land cover types after calibration using ground measurements, while the latter showed successful SM retrievals using an h-parameter of 0.1 and b-parameters of 0.174 ($\omega = 0.04$) for corn and 0.438 ($\omega = 0.07$) for soybean based on the values presented in Jackson and O'Neill (1990).

This study focused on calibration of the b and h parameters, both of which were found to be the relatively more sensitive parameters in the model compared to ω (Panciera et al., 2009a; Seo et al., 2010; Wigneron et al., 2011). Njoku and Li (1999) suggested that ω may also have dependency on VWC, but the impact on TB should be small compared to the effect of VWC on τ. Fig. 6 shows an example of the impact that ω has on the magnitude of b. For example, for $h = 0.5$ and SM = 0.2 m^3/m^3, the b-parameter would be 0.15 for $\omega = 0$ and 0.20 for $\omega = 0.05$, but the solution would not exist for $\omega = 0.10$. In the calibration, the desire was to choose the ω value that allows a solution consistent with values presented in the literature. Pellarin et al. (2006) suggested that for cropland and grassland, ω ranges from 0.06 to 0.12 for C-band and 0.08–0.12 for X-band. The SMAP SCA algorithm uses 0.05 for ω over croplands and grasslands (Chan et al., 2016), while ω varies from 0.05 to 0.12 in the mainstream L-band SM retrieval algorithms; see Table S1 in Li et al. (2022). Therefore, we assumed $\omega = 0.05$ for L-band, and $\omega = 0.08$ for both C- and X-band. The calibrated h and b values are tied to these selected ω values. Other input parameters, such as soil classification, are given in Table 2.

Parameters b and h are calibrated simultaneously through two steps: 1) pre-set ranges of 0–1.5 for b and 0–2 for h with a 0.01 interval, then retrieval of SM using all combinations of b and h by minimizing the cost function (CF):

$$\mathrm{CF} = \sum \left(TB_{sim} - TB_{obs}\right)^2, \tag{1}$$

where TB_{sim} and TB_{obs} are simulated and observed TB; and 2) determine the optimum combination of b and h with the smallest root-mean-squared-difference (RMSD) between retrieved and in situ SM:

$$\mathrm{RMSD} = \sqrt{\frac{\sum \left(SM_{ret} - SM_{obs}\right)^2}{N}}, \tag{2}$$

where SM_{ret} and SM_{obs} are retrieved and in situ observed SM, N is the number of SM data points in the time series.

Because of the coupling of b and h mentioned earlier the calibration procedure resulted in 'parallel' solutions of b and h which produced a very similar RMSD, with the difference ranging within 0.001–0.005 m^3/m^3. Therefore, in order to make a distinction between close parallel solutions from the calibration procedure, the unbiased RMSD (ubRMSD) was considered as a secondary selection criterion: for any other set of b and h that gives an RMSD no larger than 0.005 m^3/m^3 than the optimum RMSD, but ubRMSD is at least 0.01 m^3/m^3 smaller, this set of b and h will

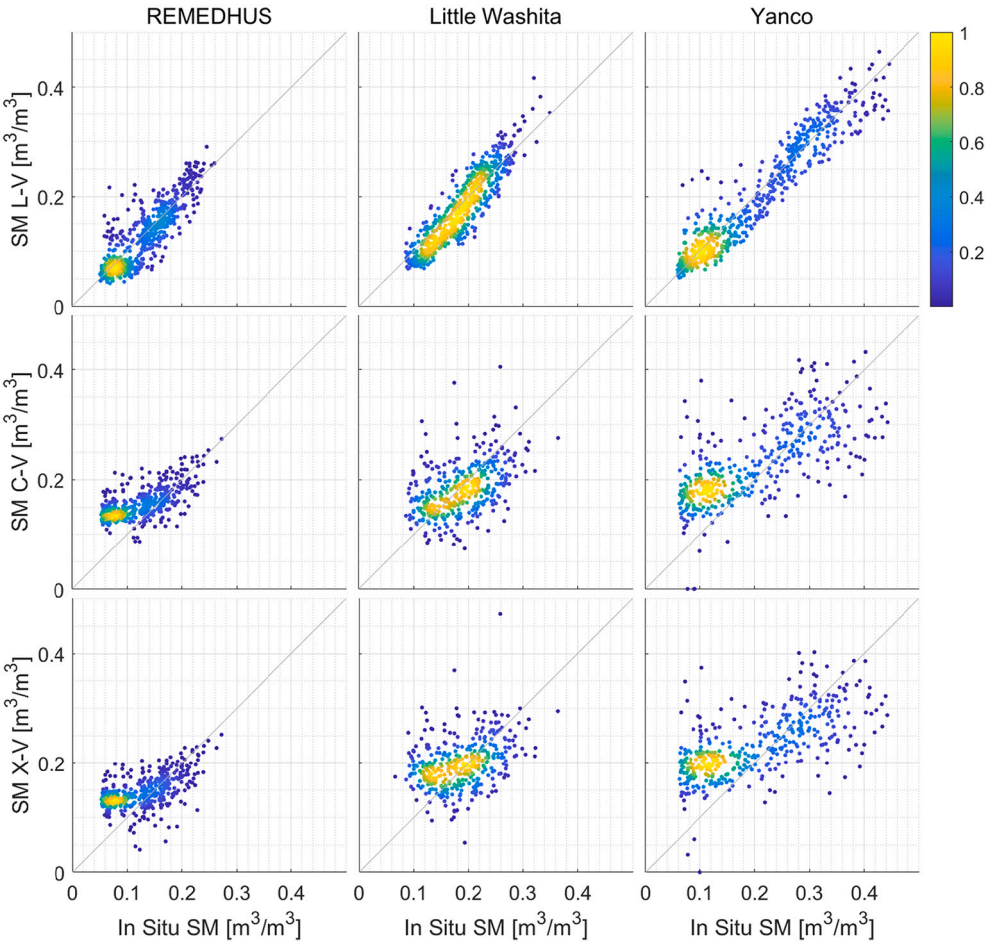

Fig. 8. Scatter plots of retrieved (x-axis) against in situ soil moisture (y-axis) at L-band, C-band and X-band at V-pol for REMEDHUS, Little Washita and Yanco for the period of 2015–2016. The colors reflect the normalized point density.

be adopted. Both parameters were calibrated for all frequencies and both polarizations. The calibrated parameters were then compared across different frequencies. SM retrieval was performed with the 2017 data set using the calibrated *b* and *h* for validation. The SMAP default parameters were also applied to compare against the result using calibrated parameters at L-band.

4. Result and discussion

4.1. Calibration

The optimized *b* and *h* parameters and their corresponding SM retrieval statistics are summarized for each site in Table 3. The best-performing statistic for each of the polarizations is marked in bold for each metric and the better of the two polarizations is additionally highlighted with red. The retrieval statistics using SMAP default parameters suggested in the ATBD for L-band analysis are also included in the table as a comparison against calibrated parameters. They were aggregated from the 1-km IGBP land cover dependent *b* and *h* parameters to the 33-km SMAP pixel.

When comparing with SMAP default parameters with the calibrated L-band parameters, *b* was smaller for most sites while *h* was larger. The calibrated parameters provide better RMSD and bias than the SMAP parameters. Conversely, the SMAP parameters provided slightly better ubRMSD for two (three) of the cropland sites, all (all) grassland sites, one (one) of the mixed sites for the V(H)-pol algorithm. Similarly, the SMAP parameter provide slightly better R for two (two) of the crop sites, one (one) grassland sites and two (one) mixed sites for the V(H)-pol algorithm. The calibration procedure seeks to optimize RMSD, which means that the result is effectively a compromise between bias and standard deviation (ubRMSD). Therefore, in many cases the calibrated result has better RMSD and bias than that of the original SMAP, which happens to achieve good ubRMSD and R with its parameterization at the expense of degraded bias.

Calibrated C- and X-band *b* parameters for all sites are generally higher than the L-band one at H-pol, but could stay similar to or even the same as the L-band one at V-pol. This would suggest that at higher frequencies vegetation effects at V-pol are not as pronounced as at H-pol. The *h* parameters at C- and X-band are significantly higher than that at L-band, especially at V-pol, while the increment at H-pol is less obvious. As discussed in Section III, it is also possible that the high *h*-parameter values compensate for the *b*-parameter values, but definitive conclusion can be not drawn.

When considering RMSD as the primary criterion, the best-performing metrics fall to L-band at V-pol, making it the ideal channel for retrieving accurate SM. Chan et al. (2016) came to a similar conclusion. For L-band, V-pol, the lowest RMSD is 0.020 m^3/m^3 for grassland, 0.029 m^3/m^3 for cropland, and 0.030 m^3/m^3 for mixed crop and grassland. Carman (cropland) stood out as a particularly problematic site and South Fork (cropland) also had considerably worse metrics compared to other sites. These are sites where the SMAP product has also challenges to meet a desirable performance standard (Chan et al., 2018). Colliander et al. (2019) investigated the retrieval issues at Carman and South Fork, and Walker et al. (2019) studied the effect of the seasonal vegetation and soil roughness cycle on the South Fork retrievals. These studies point to deficiencies in the SCA parameterization

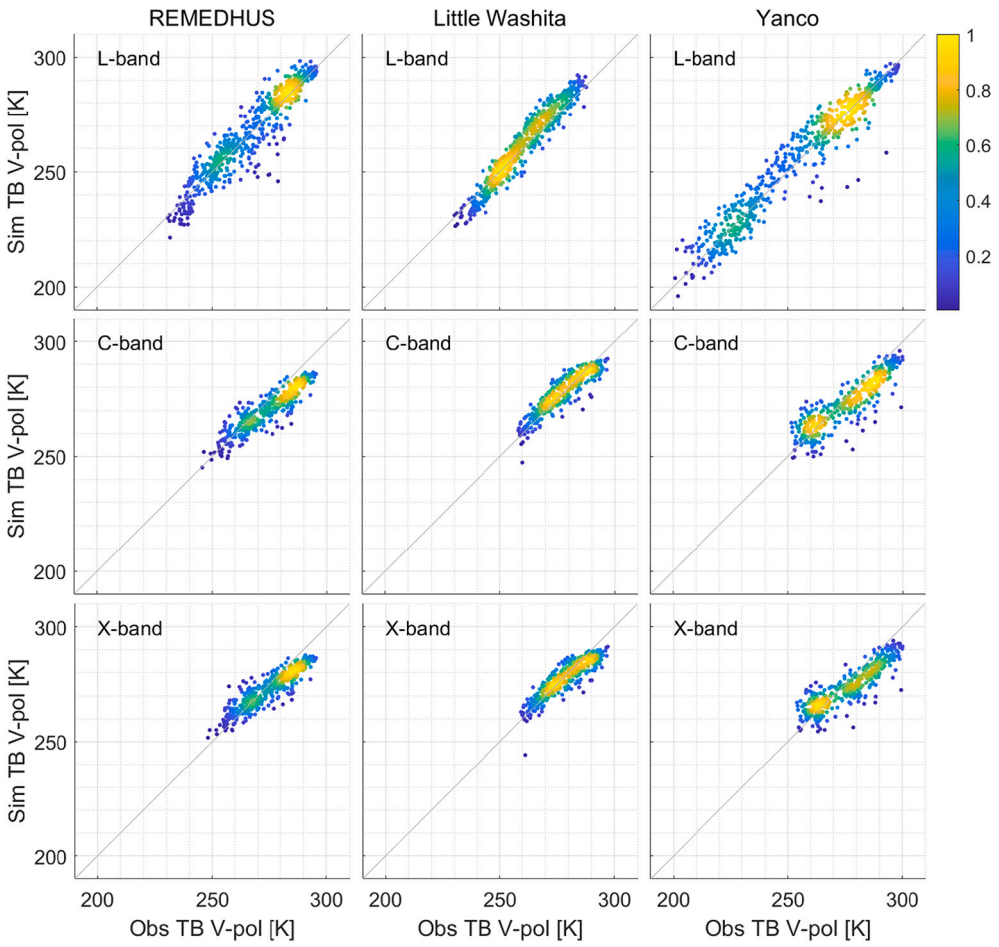

Fig. 9. Scatter plots of simulated TB using calibrated parameters against observed TB at L-band, C-band and X-band at V-pol for REMEDHUS, Little Washita and Yanco for the period of 2015–2016. The colors reflect the normalized point density.

to account the conditions at these sites. For C- and X- band V(H)-pol RMSD ranges from 0.030 (0.040) m^3/m^3 to 0.111 (0.172) m^3/m^3. It is noteworthy that even with the site-specific parameter tuning, the result at C- and X-band were not satisfactory for several of the sites. For example, for Reynolds Creek (grasslands) R indicated virtually no skill.

At L-band, the calibrated b (0.02–0.12) appears to be lower as compared to the SMAP default value of 0.11–0.13 (weighted average based on IGBP landcover map for each site), and also lower than b values suggested in Colliander et al. (2016) for grassland and cropland (0.08–0.25). The calibrated h parameter (0.19–1.11), however, has a significantly larger range than the SMAP default values (0.108–0.155), but is reasonable compared with the suggested values in previous studies (Panciera et al., 2009a; Panciera et al., 2009b; Saleh et al., 2009; Wigneron et al., 2007). The high h values may be a result of compensating low values of b or the choice of ω as shown by Fig. 10.

Fig. 7 shows the time series of the retrieved SM with the above calibrated parameters at V-pol for L-, C- and X-band for REMEDHUS, Little Washita and Yanco, in comparison with in situ SM observation during the calibration period 2015–2016. L-band retrievals capture the full dynamic range and seasonal variability of the in situ SM throughout the study period. C- and X-band retrievals, however, appear less dynamic and without clear seasonal fluctuation, especially at Little Washita. The C- and X-band retrievals underestimated SM condition during the wet season and overestimated it during the dry season.

Scatter plots presented in Fig. 8 tell a similar story. For REMEDHUS (croplands) and Yanco (mixed land cover), the SM retrieved at C-band and X-band tends to be wet-biased when SM < 0.2 m^3/m^3, and dry-biased when SM > 0.2 m^3/m^3. Among the three categories, the retrieval is least scattered for REMEDHUS (croplands).

Fig. 9 shows the simulated TB using calibrated parameters against the observed TB at L-band, C-band and X-band at V-pol for REMEDHUS, Little Washita and Yanco. This shows that as the calibration minimizes the RMSD in SM, the simulated and observed TB match each other well (RMSD: 4.4 K–6.7 K; R: 0.89–0.97). As indicated by the overall higher emissivity (Fig. 4), a larger relative portion of the TB range is a direct consequence of the variability in the physical temperature at C- and X-band than at L-band. This is one of the reasons why it is beneficial to conduct the calibration in SM space as opposed to TB space, because then the physical temperature variations (rather than the desired SM variations) cannot dominate the parameter optimization.

Calibrated b and h parameters are plotted against frequency in Fig. 10 and Fig. 11, respectively. At L-band, parameters of H-pol and V-pol cover a relatively small range across the land cover types. As the frequency increases, except for TxSON and Yanco, b increases significantly at H-pol and a little at V-pol. For the h parameter, it appears that there is an increasing relationship against frequency for both H- and V-pol. The slope from L-band to C-band was generally larger than from C-band to X-band. The exceptions are the V-pol values for Kenaston and REMEDHUS where the h parameter remained constant over frequency. While the increment at H-pol reaches to around 3–4 at X-band, the maximum roughness parameters is slightly larger than 2 at V-pol at X-band. As Fig. 10 shows, the h values are affected by the choice of ω, but the high values of h are regardless problematic for the SM retrieval because they suppress the effect of soil emissivity changes on the observed TB and therefore the effect of SM. And it appears the optimization has the tendency to favor this suppression, which does not bode

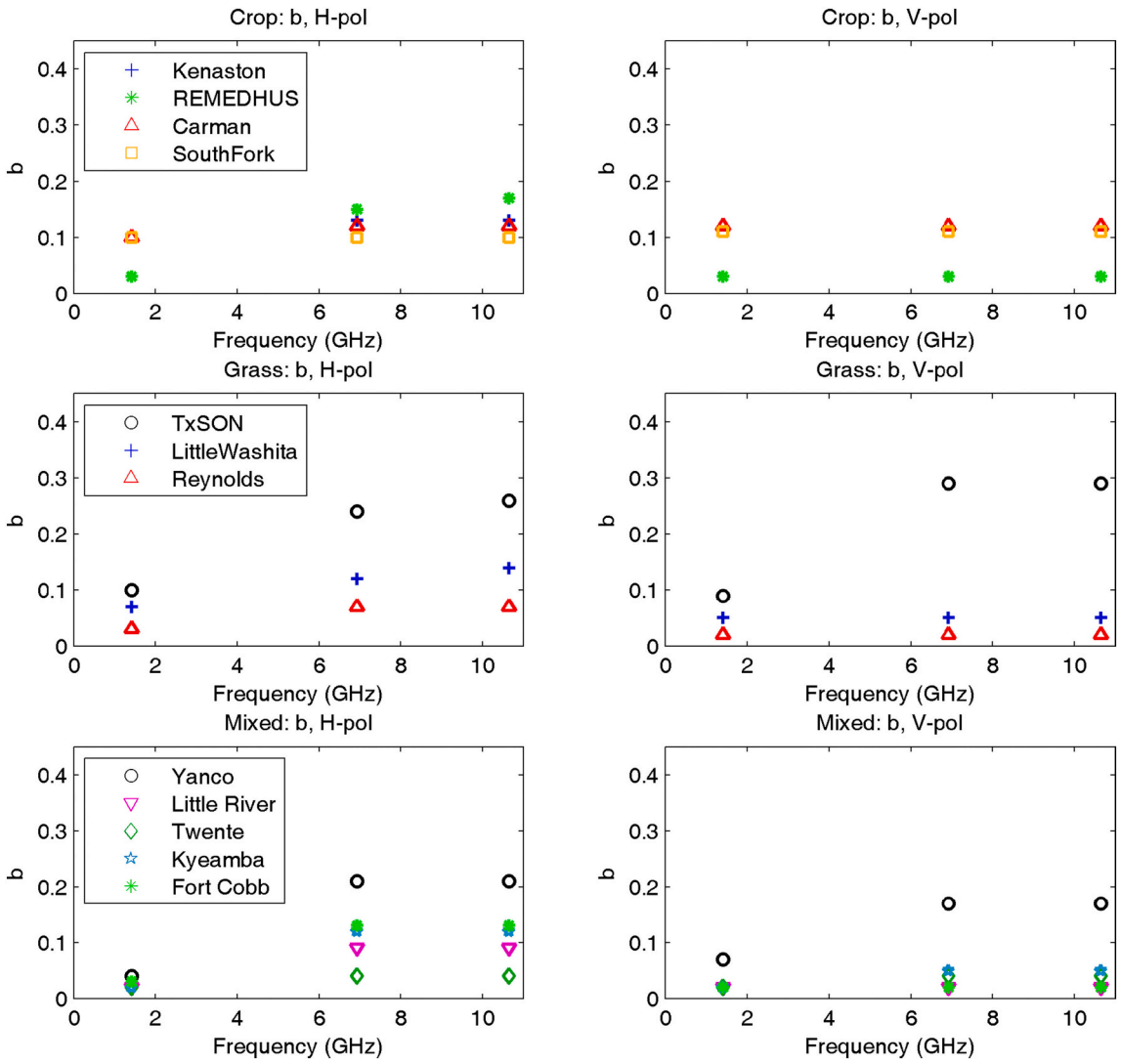

Fig. 10. Calibrated vegetation parameter b for H-pol (left) and V-pol (right) for L-, C-, and X-band at core validation sites.

well for SM retrieval. This is a further indication that the C- and X-band TB is dominated by the surface temperature instead of SM to a degree that makes an accurate SM retrieval challenging, at least with SCA-type approach.

4.2. Validation

Table 4 shows the validation statistics of the SM retrieval using the calibrated parameters for L-, C- and X-band over the year of 2017, including the retrieval statistics with the SMAP default parameters for L-band as a comparison. It can be seen from the table that for L-band, except for Twente, in which SMAP default parameters outperform the calibration by approximately 0.01 m^3/m^3 in terms of RMSD at both H- and V-pol, our calibrated retrieval for all other sites improved the RMSD by 0.002–0.037 m^3/m^3 at V-pol, and by 0.004–0.041 m^3/m^3 at H-pol. The SMAP parameters have a superior performance in unbiased RMSD at some of the grassland or cropland sites, while their corresponding biases are relatively large (0.021–0.068 m^3/m^3). In most cases, the R values were very comparable further emphasizing the point that while the parametrization improved the bias and RMSD, the parameterization has only a limited impact on the SM measurement sensitivity. One exception to this rule is Kenaston (crop lands) where the parameterization also improved R substantially.

For C- and X-band, the retrieval performance in the validation period was similar to the performance during the calibration period. The V(H)-pol ubRMSD ranged from 0.030 (0.044) to 0.091 (0.121) m^3/m^3 as compared with 0.030 (0.039) to 0.109 (0.120) m^3/m^3 during the calibration process. As expected, the L-band retrieval outperformed the C- and X-band retrieval based on all metrics. Table 5 shows the averaged validation metrics across all sites. For example, the average R for parameterized L-band V(H)-pol retrieval was 0.81 (0.77) whereas it was 0.52 (0.54) and 0.45 (0.47) for the C- and X-band, respectively. The outperformance at L-band confirms its better overall sensitivity to SM discussed in Section II·B and reported in theoretical and experimental studies in literature (e.g., Schmugge et al., 1986; Ulaby et al., 1996; Al-Yaari et al., 2019). Between the C- and X-band performance, R was slightly in favor of C-band (as expected because of the longer wavelength), but otherwise there was no practical difference in the metrics. In general, R was remarkably low for both the C- and X-band retrievals.

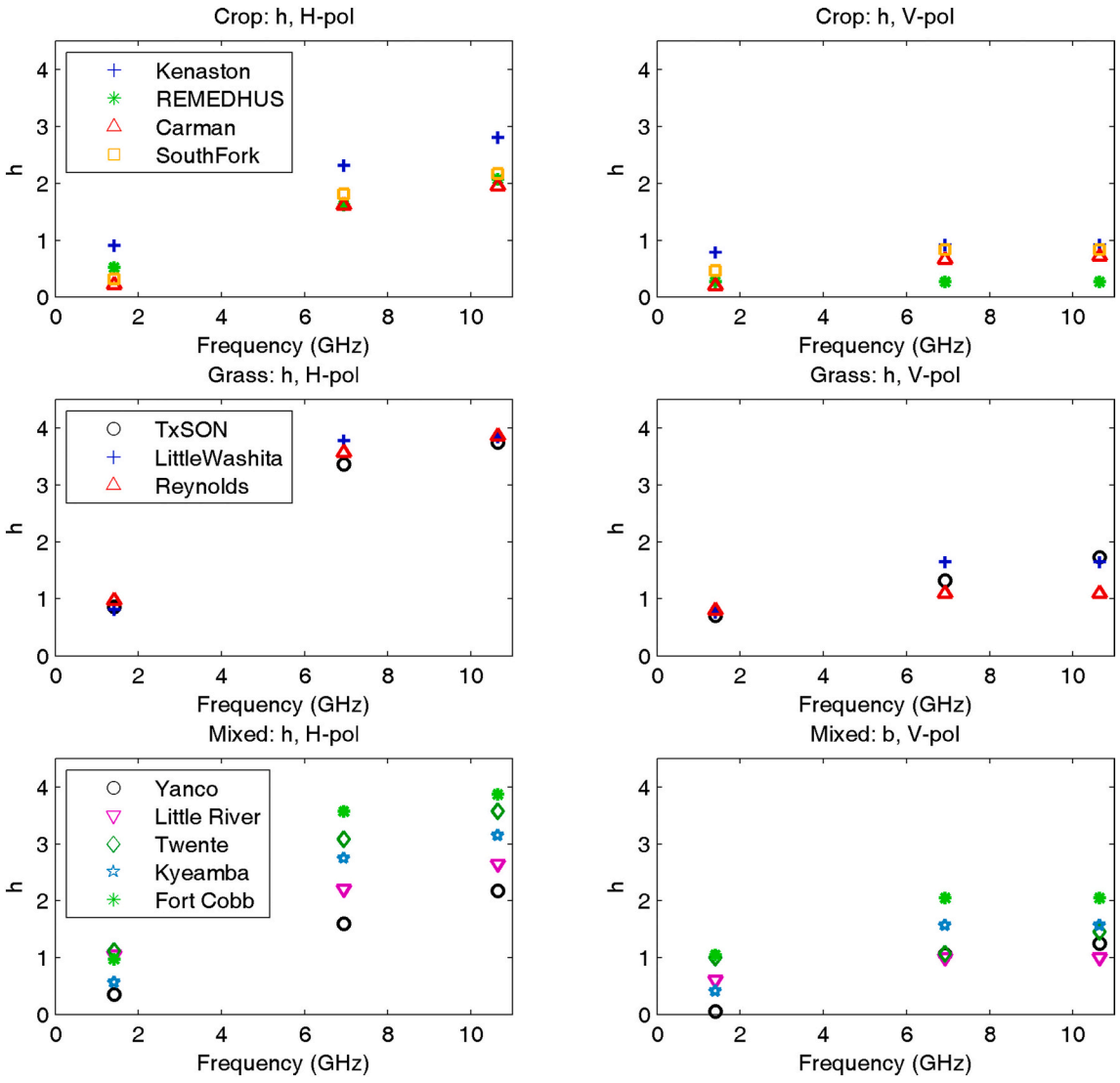

Fig. 11. Calibrated roughness parameter h for H-pol (left) and V-pol (right) for L-, C-, and X-band at core validation sites.

Table 4
Validation statistics of retrieved against in situ soil moisture using calibrated b and h for Year 2017.

Band, Pol.	b	h	RMSD	Mean Dif.	ub. RMSD	R	Band, pol	b	h	RMSD	Mean Dif.	ub. RMSD	R
CARMAN (Crop)							**KENASTON (Crop)**						
SMAP, H	*0.110*	*0.108*	*0.114*	*−0.034*	*0.109*	*0.62*	*SMAP, H*	*0.110*	*0.109*	*0.056*	*−0.046*	***0.031***	*0.69*
L-band, H	0.10	0.21	**0.110**	**−0.032**	**0.106**	**0.63**	L-band, H	0.03	0.91	**0.039**	**−0.014**	0.036	**0.81**
C-band, H	0.12	1.61	0.158	−0.134	0.121	0.17	C-band, H	0.13	2.31	0.067	−0.034	0.058	0.46
X-band, H	0.12	1.95	0.145	−0.114	0.115	0.13	X-band, H	0.13	2.80	0.074	−0.041	0.062	0.44
SMAP, V	*0.110*	*0.108*	*0.074*	*−0.021*	***0.069***	***0.68***	*SMAP, V*	*0.110*	*0.109*	*0.037*	*−0.026*	*0.027*	*0.79*
L-band, V	0.12	0.19	**0.072**	**−0.003**	0.072	0.66	L-band, V	0.03	0.78	**0.026**	−0.003	**0.026**	**0.86**
C-band, V	0.12	0.65	0.089	−0.024	0.081	0.29	C-band, V	0.03	0.92	0.030	**−0.002**	0.030	0.65
X-band, V	0.12	0.71	0.091	−0.028	0.085	0.27	X-band, V	0.03	0.92	0.032	−0.008	0.031	0.60
REMEDHUS (Crop)							**SOUTH FORK (Crop)**						
SMAP, H	*0.110*	*0.109*	***0.053***	***−0.024***	*0.047*	***0.65***	*SMAP, H*	*0.110*	*0.108*	*0.099*	*−0.059*	***0.080***	*0.68*
L-band, H	0.03	0.51	0.054	−0.032	**0.043**	0.63	L-band, H	0.10	0.31	**0.101**	**−0.038**	0.093	**0.69**
C-band, H	0.15	1.62	**0.053**	−0.008	0.052	0.64	C-band, H	0.10	1.81	0.165	−0.123	0.111	0.42
X-band, H	0.17	2.07	0.055	−0.010	0.048	0.53	X-band, H	0.10	2.17	0.159	−0.105	0.120	0.40
SMAP, V	*0.110*	*0.109*	*0.049*	*−0.010*	*0.048*	***0.69***	*SMAP, V*	*0.110*	*0.108*	***0.080***	*−0.058*	***0.056***	***0.80***
L-band, V	0.03	0.26	**0.044**	**−0.009**	**0.043**	0.68	L-band, V	0.11	0.46	**0.080**	−0.022	0.078	0.78
C-band, V	0.03	0.26	0.074	0.036	0.066	0.48	C-band, V	0.11	0.83	0.085	−0.031	0.079	0.43
X-band, V	0.03	0.26	0.074	0.038	0.067	0.42	X-band, V	0.11	0.83	0.092	**−0.013**	0.091	0.38
LITTLE WASHITA (Grass)							**REYNOLDS CREEK (Grass)**						
SMAP, H	*0.130*	*0.155*	*0.073*	*−0.069*	***0.022***	***0.88***	*SMAP, H*	*0.129*	*0.155*	*0.093*	*−0.080*	***0.048***	***0.66***
L-band, H	0.07	0.81	**0.038**	**−0.007**	0.028	0.86	L-band, H	0.02	1.10	**0.059**	−0.028	0.053	0.62
C-band, H	0.12	3.78	0.051	−0.018	0.048	0.72	C-band, H	0.12	2.70	0.085	**−0.017**	0.073	0.42
X-band, H	0.14	3.84	0.058	−0.038	0.044	0.67	X-band, H	0.12	2.80	0.088	−0.020	0.085	0.40
SMAP, V	*0.130*	*0.155*	*0.041*	*−0.035*	***0.020***	***0.90***	*SMAP, V*	*0.129*	*0.155*	*0.081*	*−0.066*	***0.047***	***0.68***
L-band, V	0.05	0.76	**0.026**	**0.000**	0.026	0.88	L-band, V	0.02	0.98	**0.053**	**−0.016**	**0.047**	0.62
C-band, V	0.05	1.65	0.042	−0.003	0.042	0.62	C-band, V	0.02	0.98	0.092	0.067	0.075	0.26
X-band, V	0.05	1.65	0.047	0.011	0.045	0.54	X-band, V	0.02	0.98	0.099	0.055	0.074	0.14
TxSON (Grass)							**FORT COBB (Mixed)**						
SMAP, H	*0.127*	*0.153*	*0.089*	*−0.087*	*0.020*	***0.91***	*SMAP, H*	*0.129*	*0.153*	*0.098*	*−0.092*	***0.034***	***0.87***
L-band, H	0.08	0.78	**0.048**	−0.044	**0.019**	**0.91**	L-band, H	0.03	0.92	**0.069**	**−0.033**	0.061	0.86
C-band, H	0.21	3.10	0.085	−0.024	0.081	0.42	C-band, H	0.10	3.60	0.089	−0.042	0.076	0.65
X-band, H	0.21	3.80	0.094	**−0.022**	0.092	0.27	X-band, H	0.10	3.92	0.098	−0.045	0.086	0.51
SMAP, V	*0.127*	*0.153*	*0.046*	*−0.042*	*0.019*	***0.91***	*SMAP, V*	*0.129*	*0.153*	*0.074*	*−0.068*	***0.031***	***0.88***
L-band, V	0.10	0.42	**0.034**	−0.029	**0.018**	**0.91**	L-band, V	0.02	0.92	**0.051**	−0.024	0.045	**0.88**
C-band, V	0.10	1.16	0.070	**0.000**	0.070	0.46	C-band, V	0.03	2.30	0.054	**−0.023**	0.053	0.46
X-band, V	0.10	1.24	0.077	−0.003	0.077	0.27	X-band, V	0.03	2.30	0.056	0.025	0.053	0.44
KYEAMBA (Mixed)							**LITTLE RIVER (Mixed)**						
SMAP, H	*0.120*	*0.135*	*0.106*	*0.042*	*0.098*	*0.82*	*SMAP, H*	*0.110*	*0.127*	*0.068*	*0.035*	*0.058*	***0.69***
L-band, H	0.02	0.56	**0.044**	**0.007**	**0.044**	**0.85**	L-band, H	0.02	1.04	**0.055**	**0.016**	**0.053**	0.64
C-band, H	0.12	2.75	0.099	−0.048	0.092	0.54	C-band, H	0.09	2.20	0.069	−0.026	0.062	0.56
X-band, H	0.12	3.15	0.102	−0.051	0.098	0.54	X-band, H	0.09	2.64	0.071	−0.025	0.064	0.50
SMAP, V	*0.120*	*0.135*	*0.097*	*0.049*	*0.083*	*0.83*	*SMAP, V*	*0.110*	*0.127*	*0.083*	*0.071*	*0.043*	***0.73***
L-band, V	0.02	0.41	**0.053**	0.025	**0.046**	**0.84**	L-band, V	0.02	0.60	**0.046**	−0.032	**0.032**	0.71
C-band, V	0.05	1.56	0.080	**−0.011**	0.079	0.44	C-band, V	0.02	1.00	0.051	0.005	0.050	0.40
X-band, V	0.05	1.56	0.085	0.022	0.083	0.45	X-band, V	0.02	1.00	0.053	**0.001**	0.053	0.31
TWENTE (Mixed)							**YANCO (Mixed)**						
SMAP, H	*0.110*	*0.120*	*0.083*	***−0.012***	*0.082*	***0.79***	*SMAP, H*	*0.122*	*0.138*	***0.028***	***−0.014***	*0.024*	***0.91***
L-band, H	0.02	1.11	0.094	−0.076	**0.055**	0.78	L-band, H	0.06	0.24	0.035	−0.028	**0.021**	**0.91**
C-band, H	0.04	3.08	0.087	−0.035	0.084	0.71	C-band, H	0.30	0.72	0.098	−0.069	0.069	0.79
X-band, H	0.04	3.57	**0.075**	−0.034	0.069	0.48	X-band, H	0.30	1.36	0.102	−0.071	0.075	0.74
SMAP, V	*0.110*	*0.120*	***0.057***	*−0.017*	*0.055*	*0.85*	*SMAP, V*	*0.122*	*0.138*	*0.029*	*0.013*	*0.026*	***0.89***
L-band, V	0.02	1.00	0.068	−0.053	**0.042**	**0.86**	L-band, V	0.06	0.06	**0.023**	**−0.006**	**0.023**	**0.89**
C-band, V	0.04	1.06	0.063	0.020	0.061	0.52	C-band, V	0.12	1.10	0.073	0.029	0.068	0.70
X-band, V	0.04	1.45	0.059	**−0.014**	0.057	0.29	X-band, V	0.12	1.22	0.079	0.031	0.073	0.64

Table 5
Averaged validation statistics across all sites.

Band, Pol.	RMSD	Mean Dif.	ubRMSD	R
SMAP, H	0.080	−0.037	0.054	0.76
L-band, H	0.062	−0.026	0.051	0.77
C-band, H	0.092	−0.048	0.077	0.54
X-band, H	0.093	−0.048	0.080	0.47
SMAP, V	0.064	−0.016	0.043	0.82
L-band, V	0.048	−0.017	0.040	0.81
C-band, V	0.066	0.004	0.062	0.52
X-band, V	0.068	0.012	0.064	0.45

5. Conclusion

This study conducted a comparison of L-, C- and X-band passive microwave observations from SMAP and AMSR2 at 12 in situ sites around the globe with grasslands, croplands or mixed of both from April 2015 to December 2017. It also presented a tau-omega model parameterization of vegetation parameter b (with a fixed ω for each frequency band) and roughness parameter h, and SM retrieval at L-, C-, and X-band at these 12 validation sites. Calibrated parameters for the C- and X-band SCA have not been available in the literature before (unlike L-band). The relationship between the parameters and frequency indicates that observations at V-pol are less sensitive to both vegetation and roughness changes as compared to H-pol. For the SM retrieval accuracy, L-band at V-pol performs the best among all channels with an ubRMSD ranging from 0.020 to 0.080 m^3/m^3. The accuracy for C- and X-band at V-pol is lower than those observed at L-band for most of the sites considered, with an overall ubRMSD range of 0.030–0.104 m^3/m^3. The validation results show that the calibration of the b and h parameters improved the L-band RMSD accuracy by 0.002–0.041 m^3/m^3 with respect to the SMAP default parameters.

The study is limited by available core validation sites. The set of sites represent the best sites that have enough SM sampling within the footprint to allow the estimation of the footprint-scale average soil moisture, but together they cover only a particular set of land cover, soil texture, hydrological and climatological conditions. Also, the time-series at the time of conducting the analysis was bounded to three growing cycles in the northern hemisphere.

Within its limitations, this study confirms earlier theoretical and experimental results that L-band SM retrieval performance is superior to C- and X-band performance. Moreover, retrieval of SM with C- and X-band is severely challenged over several sites, even with the site-specifically calibration of parameters, at least when using an SCA highlighting the importance for the continuity of L-band TB measurements to enable continuity of global high-quality SM retrievals. Nevertheless, the derived parameter combinations (h, b, ω) for each frequency can be used as a starting point for global SM retrieval algorithms, using either one of the frequencies or a combination of them. The work is also applicable to longer time-series data available from SMOS and AMSR-E dating back to 2002. In the future, missions such as CIMR (Copernicus Imaging Microwave Radiometer; Donlon, 2020) are expected to continue the L-, C- and X-band measurements, making them simultaneously and adding further potential for using them together in a complementary fashion accounting for the strengths and weaknesses of each frequency.

CRediT authorship contribution statement

Y. Gao: Methodology, Formal analysis, Software, Writing – original draft. **A. Colliander:** Conceptualization, Supervision, Methodology, Formal analysis, Software, Writing – review & editing, Project administration, Funding acquisition. **M.S. Burgin:** Conceptualization, Methodology, Software, Data curation, Writing – review & editing. **J.P. Walker:** Investigation, Data curation, Writing – review & editing. **E. Dinnat:** Conceptualization, Writing – review & editing. **C. Chae:** Conceptualization, Writing – review & editing. **M.H. Cosh:** Investigation, Data curation. **T.G. Caldwell:** Investigation, Data curation. **A. Berg:** Investigation, Data curation. **J. Martinez-Fernandez:** Investigation, Data curation. **M. Seyfried:** Investigation, Data curation. **P.J. Starks:** Investigation, Data curation. **D.D. Bosch:** Investigation, Data curation. **H. McNairn:** Investigation, Data curation. **Z. Su:** Investigation, Data curation. **R. van der Velde:** Investigation, Data curation.

Declaration of Competing Interest

The authors declare that they have no known competing financial interests or personal relationships that could have appeared to influence the work reported in this paper.

Acknowledgment

This work was carried out in part at Jet Propulsion Laboratory, California Institute of Technology under a contract with National Aeronautics and Space Administration. The University of Salamanca team involvement in this study was supported by the Spanish Ministry of Economy and Competitiveness with the project PID2020-114623RB-C33, and the European Regional Development Fund (ERDF). The contribution of University of Twente and Z. Su and R. van der Velde was (partially) funded by NWO Science domain (NWO-ENW), project <ENWWW.2018.5>. The operation of the Kenaston network is funded from Environment and Climate Change Canada and the Canadian Space Agency; Tracy Rowlandson and Erica Tetlock are acknowledged for their work with data and network operation. USDA is an equal opportunity provider and employer. This research was supported in part by the U.S. Department of Agriculture, Agricultural Research Service. USDA is an equal opportunity provider and employer. This research was a contribution from the USDA Long-Term Agroecosystem Research (LTAR) network.

References

Al-Yaari, A., Wigneron, J.-P., Dorigo, W., Colliander, A., Pellarin, T., Hahn, S., Mialon, A., Richaume, P., Fernandez-Moran, R., Fan, L., Kerr, Y.H., De Lannoy, G., 2019. Assessment and inter-comparison of recently developed/reprocessed microwave satellite soil moisture products using ISMN ground-based measurements. Remote Sens. Environ. 224, 289–303. https://doi.org/10.1016/j.rse.2019.02.008.

Bhuiyan, H.A., McNairn, H., Powers, J., Friesen, M., Pacheco, A., Jackson, T.J., Cosh, M. H., Colliander, A., Berg, A., Rowlandson, T., Bullock, P., Magagi, R., 2018. Assessing SMAP soil moisture scaling and retrieval in the Carman (Canada) study site. Vadose Zone J. 17 (1–14), 180132 https://doi.org/10.2136/vzj2018.07.0132.

Bindlish, R., Jackson, T.J., Gasiewski, A.J., Klein, M., Njoku, E.G., 2006. Soil moisture mapping and AMSR-E validation using the PSR in SMEX02. In: Remote Sensing of Environment, vol. 103, Issue 2. Elsevier BV, pp. 127–139. https://doi.org/10.1016/j.rse.2005.02.003.

Bosch, D.D., Sheridan, J.M., Lowrance, R.R., Hubbard, R.K., Strickland, T.C., Feyereisen, G.W., Sullivan, D.G., 2007. Little River experimental watershed database. Water Resour. Res. 43, W09472. https://doi.org/10.1029/2006WR005844.

Burke, W.J., Schmugge, T., Paris, J.F., 1979. Comparison of 2.8-cm and 21-cm Micorwave radiometer observations over soils with emission model calculations. J. Geophys. Res. Ocean Atmos. 84, 287–294.

Caldwell, T.G., Bongiovanni, T., Cosh, M.H., Jackson, T.J., Colliander, A., Abolt, C.J., Casteel, R., Larson, T., Scanlon, B.R., Young, M.H., 2019. The Texas soil observation network: a comprehensive soil moisture dataset for remote sensing and land surface model validation. Vadose Zone J. Accepted Paper. https://doi.org/10.2136/vzj2019.04.0034.

Chai, L., Zhang, Q., Shi, J., Liu, S., Zhao, S., Jiang, H., 2018. A parameterized multiangular microwave emission model of L-, C-, and X-bands for corn considering multiple-scattering effects. IEEE Geosci. Remote Sens. Lett. 15, 1249–1253.

Chan, S.K., Bindlish, R., O'Neill, P.E., Njoku, E., Jackson, T., Colliander, A., Chen, F., Burgin, M., Dunbar, S., Piepmeier, J., Yueh, S., Entekhabi, D., Cosh, M.H., Caldwell, T., Walker, J., Wu, X.L., Berg, A., Rowlandson, T., Pacheco, A., McNairn, H., Thibeault, M., Martinez-Fernandez, J., Gonzalez-Zamora, A., Seyfried, M., Bosch, D., Starks, P., Goodrich, D., Prueger, J., Palecki, M., Small, E.E., Zreda, M., Calvet, J.C., Crow, W.T., Kerr, Y., 2016. Assessment of the SMAP passive soil moisture product. IEEE Trans. Geosci. Remote Sens. 54, 4994–5007.

Chan, S., Bindlish, R., O'Neill, P.E., Jackson, T.J., Njoku, E., Dunbar, R.S., Chaubell, J., Peipmeier, J., Yueh, S., Entekhabi, D., Colliander, A., Chen, F., Cosh, M.H., Caldwell, T., Walker, J., Berg, A., McNairn, H., Thibeault, M., Martinez-Fernandez, J., Udall, F., Seyfried, M.S., Bosch, D.D., Starks, P., Holyfield Collins, C.,

Prueger, J.H., 2018. Development and assessment of the SMAP enhanced passive soil moisture product. Remote Sens. Environ. 204, 931–941.
Choudhury, B.J., Schmugge, T.J., Chang, A., Newton, R.W., 1979. Effects of surface roughness on the microwave emission from soils. J. Geophys. Res. 84 (C9), 5699–5706.
Colliander, A., Njoku, E.G., Jackson, T.J., Chazanoff, S., McNairn, H., Powers, J., Cosh, M.H., 2016. Retrieving soil moisture for non-forested areas using PALS radiometer measurements in SMAPVEX12 field campaign. Remote Sens. Environ. 184, 86–100.
Colliander, A., Cosh, M.H., Misra, S., Jackson, T.J., Crow, W.T., Powers, J., McNairn, H., Bullock, P., Berg, A., Magagi, R., Gao, Y., Bindlish, R., Williamson, R., Ramos, I., Latham, B., O'Neill, P., 2019. Comparison of high-resolution airborne soil moisture retrievals to SMAP soil moisture during the SMAP validation experiment 2016 (SMAPVEX16). Remote Sens. Environ. 227, 137–150. https://doi.org/10.1016/j.rse.2019.04.004.
Colliander, A., Jackson, T.J., Bindlish, R., Chan, S., Das, N., Kim, S.B., Cosh, M.H., Dunbar, R.S., Dang, L., Pashaian, L., Asanuma, J., Aida, K., Berg, A., Rowlandson, T., Bosch, D., Caldwell, T., Caylor, K., Goodrich, D., Al Jassar, H., Lopez-Baeza, E., Martinez-Fernandez, J., Gonzalez-Zamora, A., Livingston, S., McNairn, H., Pacheco, A., Moghaddam, M., Montzka, C., Notarnicola, C., Niedrist, G., Pellarin, T., Prueger, J., Pulliainen, J., Rautiainen, K., Ramos, J., Seyfried, M., Starks, P., Su, Z., Zeng, Y., van der Velde, R., Thibeault, M., Dorigo, W., Vreugdenhil, M., Walker, J.P., Wu, X., Monerris, A., O'Neill, P.E., Entekhabi, D., Njoku, E.G., Yueh, S., 2017. Validation of SMAP surface soil moisture products with core validation sites. Remote Sens. Environ. 191, 215–231.
Colliander, A., Jackson, T.J., Chan, S.K., O'Neill, P., Bindlish, R., Cosh, M.H., Caldwell, T., Walker, J.P., Berg, A., McNairn, H., Thibeault, M., Martinez-Fernandez, J., Jensen, K.H., Asanuma, J., Seyfried, M.S., Bosch, D.D., Starks, P.J., Holifield Collins, C., Prueger, J.H., Su, Z., Lopez-Baeza, E., Yueh, S.H., 2018. An assessment of the differences between spatial resolution and grid size for the SMAP enhanced soil moisture product over homogeneous sites. Remote Sens. Environ. 207, 65–70.
Colliander, A., Reichle, R., Crow, W., Cosh, M.H., Chen, F., Chan, S.K., Das, N.N., Bindlish, R., Chaubell, M.J., Kim, S., Liu, Q., Oneill, P.E., Dunbar, S., Dang, L.B., Kimball, J.S., Jackson, T.J., Aljassar, H.K., Asanuma, J., Bhattacharya, B.K., Yueh, S. H., 2022. Validation of soil moisture data products from the NASA SMAP mission. IEEE J. Sel. Top. Appl. Earth Obs. Remote Sens. https://doi.org/10.1109/jstars.2021.3124743.
Coopersmith, E., Cosh, M.H., Petersen, W.A., Prueger, J.H., Niemeier, J.J., 2015. Soil moisture model calibration and validation: an ARS watershed on the South Fork Iowa River. J. Hydrometeorol. 16, 1087–1101.
Crow, W.T., Chen, F., Reichle, R.H., Liu, Q., 2017. L-band microwave remote sensing and land data assimilation improve the representation of pre-storm soil moisture conditions for hydrologic forecasting. Geophys. Res. Lett. 44, 5495–5503. https://doi.org/10.1002/2017GL073642.
Dong, J., Crow, W.T., 2018. Use of satellite soil moisture to diagnose climate model representations of European soil moisture-air temperature coupling strength. Geophys. Res. Lett. 45, 12884–12891. https://doi.org/10.1029/2018GL080547.
Donlon, C. (Ed.), 2020. Copernicus Imaging Microwave Radiometer (CIMR) Mission Requirements Document, Version 4, ref. ESA-EOPSM-CIMR-MRD-3236. European Space Agency, Noordwijk, The Netherlands available from the.
Dorigo, W., Wagner, W., Albergel, C., Albrecht, F., Balsamo, G., Brocca, L., Chung, D., Ertl, M., Forkel, M., Gruber, A., Haas, E., Hamer, P.D., Hirschi, M., Ikonen, J., de Jeu, R., Kidd, R., Lahoz, W., Liu, Y.Y., Miralles, D., Mistelbauer, T., Nicolai-Shaw, N., Parinussa, R., Pratola, C., Reimer, C., van der Schalie, R., Seneviratne, S.I., Smolander, T., Lecomte, P., 2017. ESA CCI soil moisture for improved earth system understanding: state-of-the art and future directions. Remote Sens. Environ. 203, 185–215.
Entekhabi, D., Njoku, E.G., O'Neill, P.E., Kellogg, K.H., Crow, W.T., Edelstein, W.N., Entin, J.K., Goodman, S.D., Jackson, T.J., Johnson, J., Kimball, J., Piepmeier, J.R., Koster, R.D., Martin, N., McDonald, K.C., Moghaddam, M., Moran, S., Reichle, R., Shi, J.C., Spencer, M.W., Thurman, S.W., Tsang, L., Van Zyl, J., 2010. The soil moisture active passive (SMAP) mission. Proc. IEEE 98, 704–716.
Entekhabi, D., Yueh, S., O'Neill, P., Kellogg, K., 2014. SMAP Handbook – Soil Moisture Active Passive: Mapping Soil Moisture and Freeze/Thaw from Space. SMAP Project. Jet Propulsion Laboratory, Pasadena, CA.
Fernandez-Moran, R., Wigneron, J.-P., De Lannoy, G., Lopez-Baeza, E., Parrens, M., Mialon, A., Mahmoodi, A., Al-Yaari, A., Bircher, S., Al Bitar, A., Richaume, P., Kerr, Y., 2017. A new calibration of the effective scattering albedo and soil roughness parameters in the SMOS SM retrieval algorithm. In: International Journal of Applied Earth Observation and Geoinformation, vol. 62. Elsevier BV, pp. 27–38. https://doi.org/10.1016/j.jag.2017.05.013.
Imaoka, K., Kachi, M., Fujii, H., Murakami, H., Hori, M., Ono, A., Igarashi, T., Nakagawa, K., Oki, T., Honda, Y., Shimoda, H., 2010. Global change observation mission (GCOM) for monitoring carbon, water cycles, and climate change. Proc. IEEE 98, 717–734.
Jackson, T.J., O'Neill, P.E., 1990. Attenuation of soil microwave emission by corn and soybeans at 1.4 GHz and 5 GHz. IEEE Trans. Geosci. Remote Sens. 28, 978–980.
Jackson, T.J., Schmugge, T.J., 1991. Vegetation effects in the microwave emission of soils. Remote Sens. Environ. 36, 203–212.
Jackson, T.J., Le Vine, D.M., Hsu, A.Y., Oldak, A., Starks, P.J., Swift, C.T., Isham, J.D., Haken, M., 1999. Soil moisture mapping at regional scales using microwave radiometry: the southern Great Plains hydrology experiment. IEEE Trans. Geosci. Remote Sens. 37 (5), 2136–2151. https://doi.org/10.1109/36.789610.
Jackson, T.J., Gasiewski, A.J., Oldak, A., Klein, M., Njoku, E.G., Yevgrafov, A., Christiani, S., Bindlish, R., 2002. Soil moisture retrieval using the C-band polarimetric scanning radiometer during the Southern Great Plains 1999 experiment. IEEE Trans. Geosci. Remote Sens. 40, 2151–2161.
Kerr, Y.H., Waldteufel, P., Wigneron, J.P., Delwart, S., Cabot, F., Boutin, J., Escorihuela, M.J., Font, J., Reul, N., Gruhier, C., Juglea, S.E., Drinkwater, M.R., Hahne, A., Martin-Neira, M., Mecklenburg, S., 2010. The SMOS mission: new tool for monitoring key elements of the global water cycle. Proc. IEEE 98, 666–687.
Kerr, Y.H., Waldteufel, P., Richaume, P., Wigneron, J.P., Ferrazzoli, P., Mahmoodi, A., Al Bitar, A., Cabot, F., Gruhier, C., Juglea, S.E., Leroux, D., Mialon, A., Delwart, S., 2012. The SMOS soil moisture retrieval algorithm. IEEE Trans. Geosci. Remote Sens. 50, 1384–1403.
Kirdiashev, K.P., Chukhlantsev, A.A., Shutko, A.M., 1979. Microwave radiation of the earth's surface in the presence of vegetation cover. Radio Eng. Electron. Phys. 24, 256–264 (Engl. transl).
Li, X., Wigneron, J.-P., Fan, L., Frappart, F., Yueh, S.H., Colliander, A., Ebtehaj, A., Gao, L., Fernandez-Moran, R., Liu, X., Wang, M., Ma, H., Moisy, C., Ciais, P., 2022. A new SMAP soil moisture and vegetation optical depth product (SMAP-IB): Algorithm, assessment and inter-comparison. In: Remote Sensing of Environment, vol. 271. Elsevier BV, p. 112921. https://doi.org/10.1016/j.rse.2022.112921.
Lv, S., Wen, J., Zeng, Y., Tian, H., Su, Z., 2014. An improved two-layer algorithm for estimating effective soil temperature in microwave radiometry using in situ temperature and soil moisture measurements. Remote Sens. Environ. 152, 356–363.
Martinez-Fernandez, J., Ceballos, A., 2005. Mean Soil Moisture Estimation Using Temporal Stability Analysis, vol. 312, pp. 28–38. https://doi.org/10.1016/j.jhydrol.2005.02.007.
Mironov, V.L., Kosolapova, L.G., Fomin, S.V., 2009. Physically and mineralogically based spectroscopic dielectric model for moisture soils. IEEE Trans. Geosci. Rem. Sens. 47 (7), 2059–2070.
Mladenova, I.E., Jackson, T.J., Njoku, E., Bindlish, R., Chan, S., Cosh, M.H., Holmes, T.R. H., de Jeu, R.A.M., Jones, L., Kimball, J., Paloscia, S., Santi, E., 2014. Remote monitoring of soil moisture using passive microwave-based techniques - theoretical basis and overview of selected algorithms for AMSR-E. Remote Sens. Environ. 144, 197–213.
Mo, T., Choudhury, B.J., Schmugge, T.J., Wang, J.R., Jackson, T.J., 1982. A model for the microwave emission of vegetation-covered fields. J. Geophys. Res. 87, 229–237.
Njoku, E.G., Kong, J.A., 1977. Theory for passive microwave remote sensing of near-surface soil moisture. J. Geophys. Res. 82, 3108–3118.
Njoku, E.G., Li, L., 1999. Retrieval of land surface parameters using passive microwave measurements at 6-18 GHz. IEEE Trans. Geosci. Remote Sens. 37, 79–93.
Njoku, E.G., Wilson, W.J., Yueh, S.H., Dinardo, S.J., Li, F.K., Jackson, T.J., Lakshmi, V., Bolten, J., 2002. Observations of soil moisture using a passive and active low-frequency microwave airborne sensor during SGP99. IEEE Trans. Geosci. Remote Sens. 40, 2659–2673.
Njoku, E.G., Jackson, T.J., Lakshmi, V., Chan, T.K., Nghiem, S.V., 2003. Soil moisture retrieval from AMSR-E. IEEE Trans. Geosci. Remote Sens. 41, 215–229.
O'Neill, P., Chan, S., Njoku, E., Jackson, T., Bindlish, R., Chaubell, J., Colliander, A., 2021. Soil Moisture Active Passive (SMAP) Algorithm Theoretical Basis Document Level 2 & 3 Soil Moisture (Passive) Data Products. Jet Propulsion Laboratory, p. 75.
O'Neill, P.E., Chauhan, N.S., Jackson, T.J., 1996. Use of active and passive microwave remote sensing for soil moisture estimation through corn. Int. J. Remote Sens. 17 (10), 1851–1865. https://doi.org/10.1080/01431169608948743.
Paloscia, S., Macelloni, G., Santi, E., Koike, T., 2001. A multifrequency algorithm for the retrieval of soil moisture on a large scale using microwave data from SMMR and SSM/I satellites. IEEE Trans. Geosci. Remote Sens. 39, 1655–1661.
Pampaloni, P., Paloscia, S., 1986. Microwave emission and plant water content: a comparison between field measurements and theory. IEEE Trans. Geosci. Remote Sens. GE-24 (6), 900–905. https://doi.org/10.1109/tgrs.1986.289705.
Panciera, R., Walker, J.P., Kalma, J.D., Kim, E.J., Saleh, K., Wigneron, J.P., 2009a. Evaluation of the SMOS L-MEB passive microwave soil moisture retrieval algorithm. Remote Sens. Environ. 113, 435–444.
Panciera, R., Walker, J.P., Merlin, O., 2009b. Improved understanding of soil surface roughness parameterization for L-band passive microwave soil moisture retrieval. IEEE Geosci. Remote Sens. Lett. 6, 625–629.
Panciera, R., Walker, J.P., Jackson, T.J., Gray, D.A., Tanase, M.A., Ryu, D., Monerris, A., Yardley, H., Rudiger, C., Wu, X., Gao, Y., Hacker, J.M., 2014. The soil moisture active passive experiments (SMAPEx): toward soil moisture retrieval from the SMAP Mission. IEEE Trans. Geosci. Remote Sens. 52 (1), 490–507. https://doi.org/10.1109/tgrs.2013.2241774.
Parinussa, R.M., Holmes, T.R.H., Wanders, N., Dorigo, W.A., de Jeu, R.A.M., 2015. A preliminary study toward consistent soil moisture from AMSR2. J. Hydrometeorol. 16, 932–947.
Pellarin, T., Kerr, Y.H., Wigneron, J.P., 2006. Global simulation of brightness temperatures at 6.6 and 10.7 GHz over land based on SMMR data set analysis. IEEE Trans. Geosci. Remote Sens. 44, 2492–2505.
Piepmeier, J.R., Focardi, P., Horgan, K.A., Knuble, J., Ehsan, N., Lucey, J., Brambora, C., Brown, P.R., Hoffman, P.J., French, R.T., Mikhaylov, R.L., Kwack, E.Y., Slimko, E.M., Dawson, D.E., Hudson, D., Peng, J., Mohammed, P.N., Amici, G.D., Freedman, A.P., Medeiros, J., Sacks, F., Estep, R., Spencer, M.W., Chen, C.W., Wheeler, K.B., Edelstein, W.N., O'Neill, P.E., Njoku, E.G., 2017. SMAP L-band microwave radiometer: instrument design and first year on orbit. IEEE Trans. Geosci. Remote Sens. 55, 1954–1966.
Saleh, K., Kerr, Y.H., Richaume, P., Escorihuela, M.J., Panciera, R., Delwart, S., Boulet, G., Maisongrande, P., Walker, J.P., Wursteisen, P., Wigneron, J.P., 2009. Soil moisture retrievals at L-band using a two-step inversion approach (COSMOS/NAFE'05 experiment). Remote Sens. Environ. 113, 1304–1312.
Schmugge, T., Oneill, P.E., Wang, J.R., 1986. Passive microwave soil-moisture research. IEEE Trans. Geosci. Remote Sens. 24, 12–22.

Seo, D., Lakhankar, T., Khanbilvardi, R., 2010. Sensitivity analysis of b-factor in microwave emission model for soil moisture retrieval: a case study for SMAP Mission. Remote Sens. 2, 1273–1286.

Seyfried, M.S., Lohse, K.A., Marks, D., Flerchinger, G.N., Pierson, F., Holbrook, S., 2018. Reynolds Creek experimental watershed and critical zone observatory. Vadoze Zone J. 17, 180129 https://doi.org/10.2136/vzj2018.07.0129.

Smith, A.B., Walker, J.P., Western, A.W., Young, R.I., Ellett, K.M., Pipunic, R.C., Grayson, R.B., Siriwardena, L., Chiew, F.H.S., Richter, H., 2012. The Murrumbidgee soil moisture monitoring network data set. Water Resour. Res. 48, W07701. https://doi.org/10.1029/2012WR011976.

Starks, P.J., Steiner, J.L., Stern, A.J., 2014. Upper Washita River experimental watersheds: land cover data sets (1974–2007) for two southwestern Oklahoma agricultural watersheds. J. Environ. Qual. 43, 1310–1318.

Tetlock, E., Toth, B., Berg, A., Rowlandson, T., Ambadan, J.T., 2019. An 11-year (2007–2017) soil moisture and precipitation dataset from the Kenaston network in the Brightwater Creek Basin, Saskatchewan, Canada. Earth Syst. Sci. Data 11 (2), 787–796. https://doi.org/10.5194/essd-11-787-2019.

Ulaby, F., Wilson, E., 1985. Microwave attenuation properties of vegetation canopies. In: IEEE Transactions on Geoscience and Remote Sensing, vol. GE-23, pp. 746–753. https://doi.org/10.1109/tgrs.1985.289393. Issue 5.

Ulaby, F., Dubois, P., van Zyl, J., 1996. Radar mapping of surface soil moisture. J. Hydrol. 184 (1–2), 57–84.

Van de Griend, A.A., Wigneron, J.P., 2004. The b-factor as a function of frequency and canopy type at h-polarization. IEEE Trans. Geosci. Remote Sens. 42, 786–794.

van der Schalie, R., de Jeu, R., Rodriguez-Fernandez, N., Al-Yaari, A., Kerr, Y., Wigneron, J.-P., Parinussa, R., Drusch, M., 2018. The effect of three different data fusion approaches on the quality of soil moisture retrievals from multiple passive microwave sensors. Remote Sens. 10 (1), 107. https://doi.org/10.3390/rs10010107.

van der Velde, R., Colliander, A., Pezij, M., Benninga, H.-J.F., Bindlish, R., Chan, S.K., Jackson, T.J., Hendriks, D.M.D., Augustijn, D.C.M., Su, Z., 2021. Validation of SMAP L2 passive-only soil moisture products using upscaled in situ measurements collected in Twente, the Netherlands. Hydrol. Earth Syst. Sci. 25 (473–495), 2021. https://doi.org/10.5194/hess-25-473-2021.

Walker, V.A., Hornbuckle, B.K., Cosh, M.H., Prueger, J.H., 2019. Seasonal evaluation of SMAP soil moisture in the U.S. Corn Belt. Remote Sens. 11 (21) https://doi.org/10.3390/rs11212488.

Wigneron, J.-P., Chanzy, A., Calvet, J.-C., Bruguier, N., 1995. A simple algorithm to retrieve soil moisture and vegetation biomass using passive microwave measurements over crop fields. Remote Sens. Environ. 51 (3), 331–341. https://doi.org/10.1016/0034-4257(94)00081-w.

Wigneron, J.-P., Laguerre, L., Kerr, Y.H., 2001. A simple parameterization of the L-band microwave emission from rough agricultural soils. IEEE Trans. Geosci. Remote Sens. 39 (8), 1697–1707. https://doi.org/10.1109/36.942548.

Wigneron, J.P., Kerr, Y., Waldteufel, P., Saleh, K., Escorihuela, M.J., Richaume, P., Ferrazzoli, P., de Rosnay, P., Gurney, R., Calvet, J.C., Grant, J.P., Guglielmetti, M., Hornbuckle, B., Matzler, C., Pellarin, T., Schwank, M., 2007. L-band microwave emission of the biosphere (L-MEB) model: description and calibration against experimental data sets over crop fields. Remote Sens. Environ. 107, 639–655.

Wigneron, J.P., Chanzy, A., Kerr, Y.H., Lawrence, H., Shi, J., Escorihuela, M.J., Mironov, V., Mialon, A., Demontoux, F., de Rosnay, P., Saleh-Contell, K., 2011. Evaluating an improved parameterization of the soil emission in L-MEB. IEEE Trans. Geosci. Remote Sens. 49, 1177–1189.

Wigneron, J.-P., Jackson, T.J., O'Neill, P., De Lannoy, G., de Rosnay, P., Walker, J.P., Ferrazzoli, P., Mironov, V., Bircher, S., Grant, J.P., Kurum, M., Schwank, M., Munoz-Sabater, J., Das, N., Royer, A., Al-Yaari, A., Al Bitar, A., Fernandez-Moran, R., Lawrence, H., Kerr, Y., 2017. Modelling the passive microwave signature from land surfaces: A review of recent results and application to the L-band SMOS & SMAP soil moisture retrieval algorithms. Remote Sens. Environ. 192, 238–262. https://doi.org/10.1016/j.rse.2017.01.024.